Xie *et al. Int J Concr Struct Mater* (2025) 19:79
https://doi.org/10.1186/s40069-025-00818-9

International Journal of Concrete Structures and Materials

RESEARCH Open Access

Experimental Research of Fatigue Performance of OSDs with Severe Fatigue Cracking After Reinforcement Using UHPC Layer

Zengkui Xie[1], Zhilin Chen[2], Chenhui Zhu[3*], Zhongsong Su[4], Lipo Yang[5] and Wei Zou[2]

Abstract

Based on the newly developed technology proposed by our team, which involves reinforcing severely cracked orthotropic steel bridge decks (OSDs) with an ultra-high-performance concrete (UHPC) layer containing transverse steel-plate strips, this study conducted full-scale fatigue performance validation tests on the steel–UHPC composite bridge deck of the Junshan Yangtze River Bridge. To verify that the observed stress distribution reasonably reflects the actual structural behavior, finite-element modeling was used to derive the stress influence lines for both the actual bridge segment model and the laboratory-test specimen designed in this study across different fatigue details. The finite-element analysis showed good agreement between the model of the actual bridge segment and that of the laboratory-test specimen. The fatigue tests were conducted in three phases. In the first phase, fatigue cracks were initiated and monitored at specific critical details of the deck before reinforcement. The results indicated that cracks formed most easily and propagated most quickly at the intersections between the deck plate and U-ribs, as well as at the weld holes between U-ribs and transverse diaphragms. In the second phase, the propagation of these fatigue cracks and the changes in stress were compared before and after the UHPC layer reinforcement. The findings proved that the UHPC layer effectively suppressed crack growth and reduced the stress amplitude at fatigue-prone details (with reductions of up to 96% at the deck plate and U-ribs, and up to 57% at the U-ribs and diaphragm weld holes). In the third phase, the model underwent additional fatigue testing, including 1 million loading cycles at the diaphragm and 2 million two-point loading cycles at the mid-span, to verify the long-term fatigue resistance of the reinforced model throughout its entire service life. Data provided by the health monitoring system of the in-situ measurements on a real bridge further validated the effectiveness of the reinforcement measures in reducing stress amplitude at fatigue-sensitive locations (with stress amplitude reductions of up to 86% at the intersections of the deck plate, U-ribs, and transverse diaphragms). This study provides actionable insights into fatigue behaviors and reinforcement strategies, contributing valuable experience toward the maintenance and preservation of similar infrastructure.

Keywords Fatigue performance, Numerical simulation, Shear connectors, Steel–UHPC composite bridge deck, Stress amplitude

*Correspondence:
Chenhui Zhu
Full list of author information is available at the end of the article

1 Introduction

Orthotropic steel decks (OSDs) have been widely adopted in long-span bridges due to their high strength-to-weight ratio and excellent structural efficiency (Structure Magazine, 2021; Shili & ZHou, 2017). However, OSDs are prone to fatigue cracking after years of heavy traffic service (Dong et al., 2020; Huang et al., 2006; Radaj et al., 2009; Samol & Yamada, 2008; Tang et al., 2012; Xiong et al., 2003). Fatigue cracks typically initiate at welded joints and other stress concentration details (e.g., deck-to-rib welds and rib-to-diaphragm connections), because repetitive vehicle loading causes large local deformations and high stress ranges (Chen, 2015; Ling & Tang, 2018; Ren et al., 2007; Tang et al., 2014; Wang, 2019; Xiong et al., 2021; Zhang et al., 2017). These cracks not only compromise the structural integrity of the bridge deck but also lead to deterioration of the pavement overlay (e.g., asphalt) due to reduced deck stiffness (Dong et al., 2020). Consequently, ensuring the fatigue durability of OSDs has become a critical concern for bridge safety and service life extension (Dong et al., 2020).

Over the past decades, researchers and engineers have investigated various remedial measures to mitigate fatigue damage in OSDs (Fu et al., 2017; Zhang et al., 2019; Short Span Steel Bridge AlLiance, 2020; Abdelbaset et al., 2022; Xin et al., 2021; Wei et al., 2022; Zhu et al., 2023; Xiang and Zhu, 2021; Li, 2018; Yiming 2019). Traditional methods include drilling stop-holes at crack tips to relieve stress intensity (Fu et al., 2017), welding additional stiffeners or cover plates at vulnerable details (Zhang et al., 2019), and introducing steel-plate–elastomer sandwich patches (SPS) on the deck (Short Span Steel Bridge AlLiance, 2020). While these techniques can slow crack growth, their effectiveness is limited—the local stiffness of the deck is only modestly improved, so new cracks may form or existing cracks may re-initiate after a relatively short period (Fu et al., 2017). In practice, many bridges reinforced by these conventional means have experienced recurrent cracking, highlighting the need for more robust strengthening solutions (Zhang et al., 2019).

In recent years, ultra-high-performance concrete (UHPC) has emerged as a promising material for strengthening orthotropic steel decks. UHPC, a fiber-reinforced cementitious composite, offers ultra-high compressive strength, excellent tensile toughness, and superior durability (Dieng et al., 2013a; Hou et al., 2025; Qin et al., 2022; Shi et al., 2022; Zhang et al., 2022). By casting a thin UHPC layer atop the steel deck (often anchored with shear connectors), a composite steel–UHPC deck can be formed, significantly increasing deck stiffness and distributing wheel loads more evenly (Dieng et al., 2013a). This composite action reduces stress amplitudes at fatigue-prone details, thereby delaying crack initiation and growth. Several studies have demonstrated the potential benefits of UHPC layers: for example, lab tests and numerical analyses have shown that adding a UHPC overlay can cut the stress range in rib-to-deck welds by 50–70%, greatly extending fatigue life (Dieng et al., 2013a; Shi et al., 2022). UHPC overlays have already been applied in new bridge constructions and pilot retrofit projects—such as the Yangtze River Bridge in China—yielding improved fatigue performance in service (Qin et al., 2022; Zhang et al., 2022).

Despite these encouraging developments, there is still a lack of full-scale experimental evidence on the efficacy of UHPC for retrofit of severely cracked OSDs (Kim et al., 2015; Dieng et al. ((Dieng, et al., 2013b)); Yang et al. ((Yang, et al., 2021)); Bing et al. ((Bing, et al., 2023)); Junhui et al. ((Junhui, et al., 2022)); (Xudong and Minghong ((Xudong, et al., 2017))) ((Xudong, and Minghong, 2019)); Xudong et al. ((Xudong, and Junhui, 2017)); Xudong et al. ((Xudong, et al., 2012)); Shao et al. ((Shao, et al., 2013)); Xudong and Junhui ((Xudong, and Junhui, 2017)); Junhui ((Junhui, et al., 2022)); Standards of the People's Republic of China: Code for Design of Highway Steel Bridges, 2015). Most existing studies focus on idealized or moderately damaged specimens, or rely on simulation, which may not capture the complex behavior of an in-service bridge (Shi et al., 2022). The fatigue performance of an OSD that has already accumulated substantial cracking, when strengthened with a UHPC layer, remains to be fully verified under realistic load conditions(Han-yong et al.

Fig. 1 Cracking condition after initial maintenance of the Junshan Yangtze River Bridge

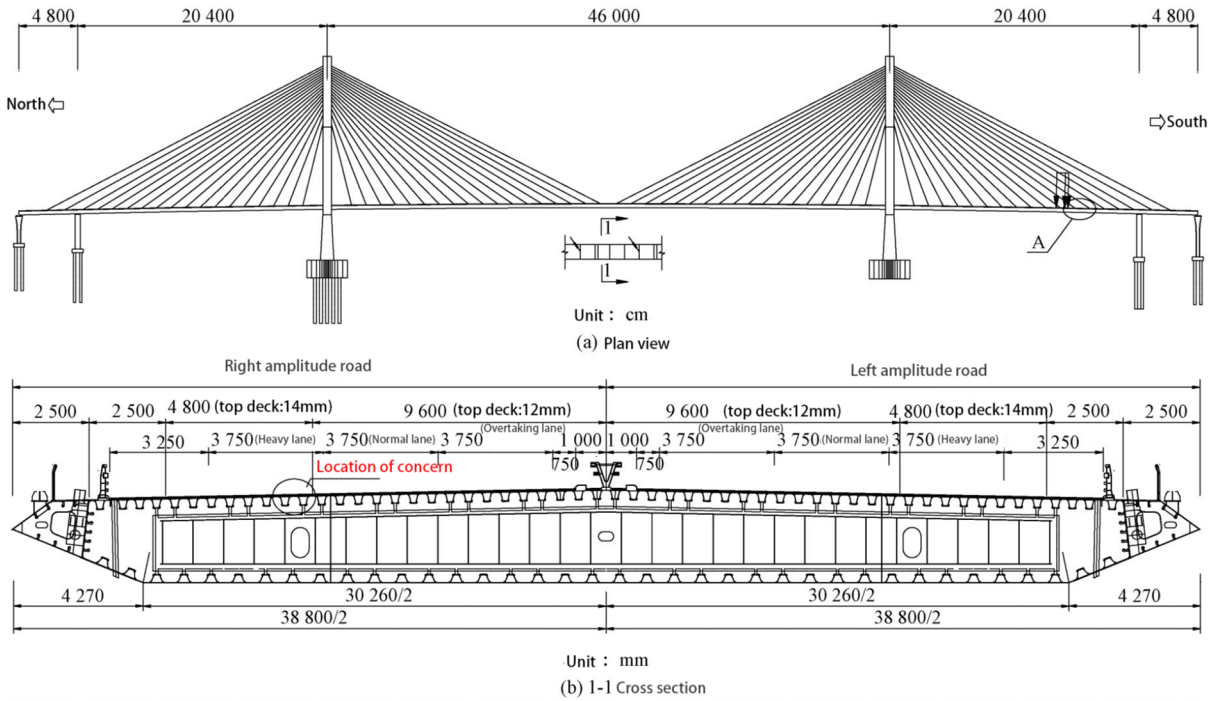

Fig. 2 Junshan Yangtze River Bridge elevation and standard section diagram

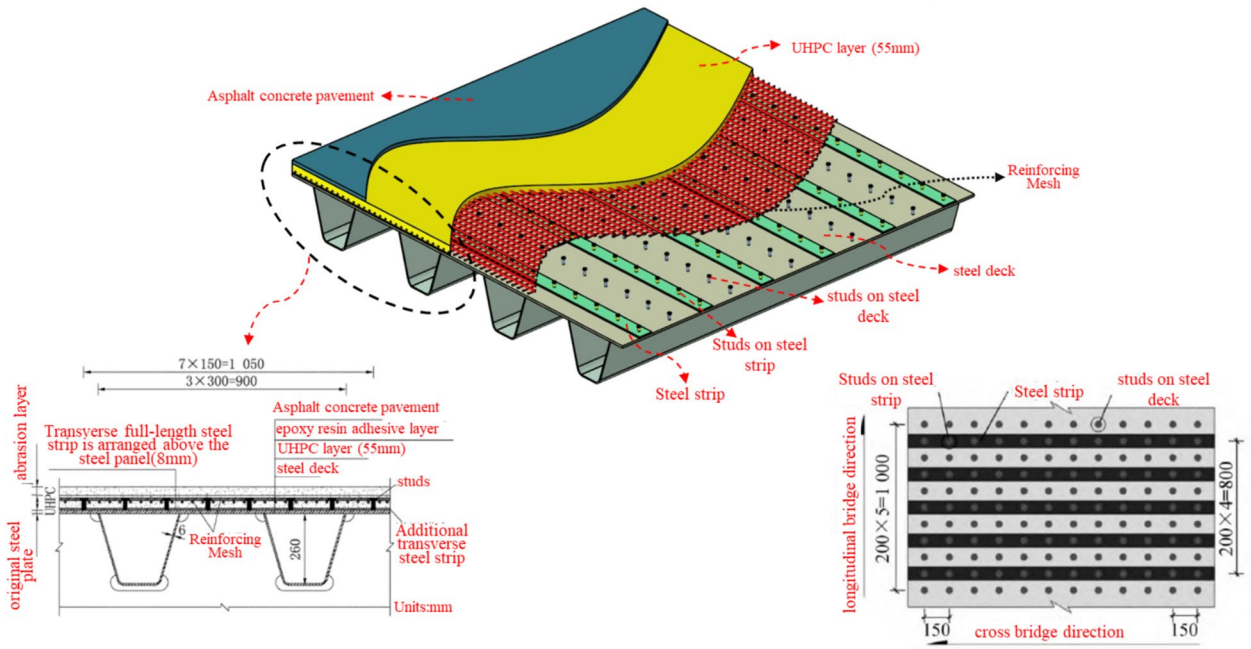

Fig. 3 Junshan Yangtze River Bridge elevation and standard section diagram

((Hanyong, et al., 2019)); Qinghua et al. ((Qinghua, et al., 2017)); Aizhu ((Aizhu, 2017)); Chunsheng et al. ((Chunsheng, et al., 2013)); Liang et al. ((Liang, et al., 2014)); Qinghua et al. ((Qinghua, et al., 2014)); Wang et al. ((Wang, et al., 2021)); (Qin et al. (Qin, et al., 2022)); (Qin, et al., 2022); Libing et al. ((Libing, et al., 2020)); Yang et al. ((Yang, et al., 2020))). Moreover, practical design details (such as how to integrate

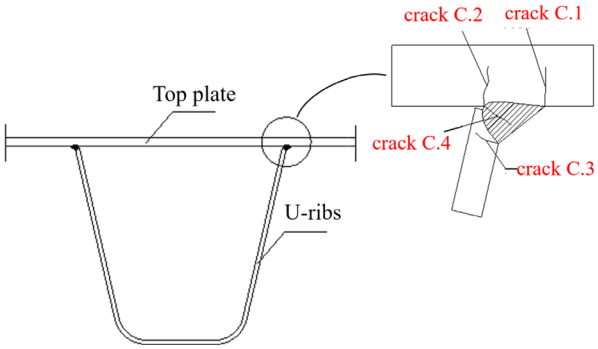

(a) In-plane crack types at the junction of the top plate and U-rib.

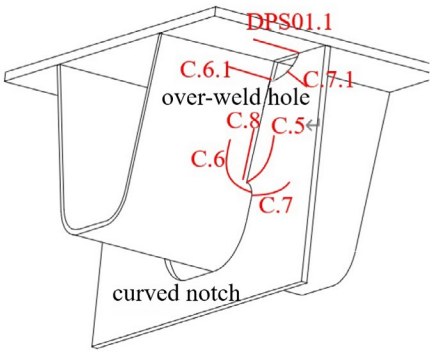

(b) Crack types near the curved notch.

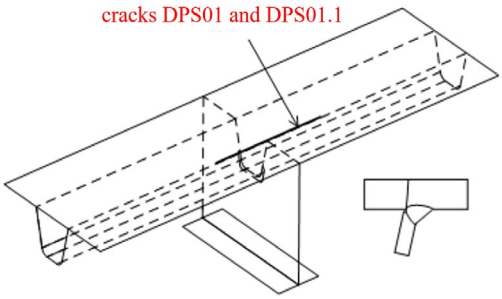

(c) Out-of-plane crack types at the junction of the transverse diaphragm, top plate, and U-rib.

Fig. 4 Schematic diagram of crack types

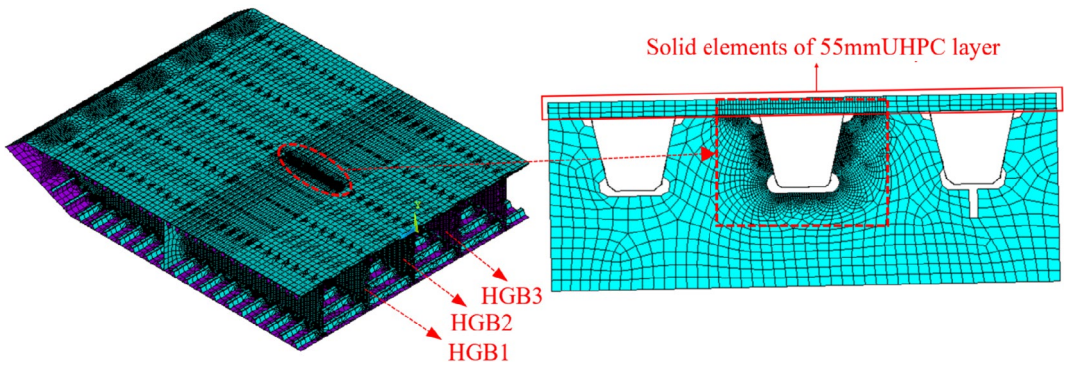

Fig. 5 Section steel box girder finite-element model and concerned area grid division after using steel–UHPC composite bridge deck reinforcement

steel-plate strips or connectors within the UHPC layer) and the long-term performance of the strengthened deck need further validation. Addressing these knowledge gaps is essential before UHPC retrofitting can be widely recommended for aging bridges with serious fatigue damage.

In this study, a newly developed UHPC layer reinforcement technique—incorporating transverse steel-plate

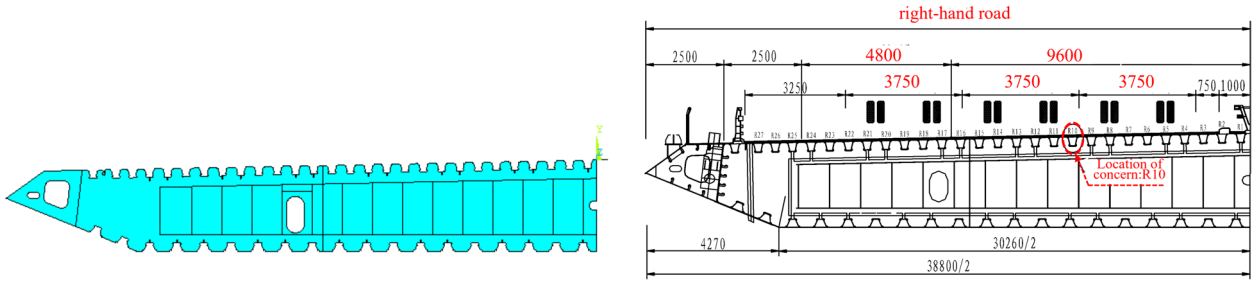

Fig. 6 Solid web diaphragm model diagram and concerned construction detail location schematic

strips embedded in the UHPC overlay—is applied to an orthotropic steel deck with severe fatigue cracks. A full-scale segment of the actual bridge deck (from the Junshan Yangtze River Bridge) was tested under cyclic loading to evaluate the fatigue performance after UHPC reinforcement. The introduction of steel strips within the UHPC layer is intended to enhance composite action and crack control, representing an innovative improvement over conventional overlays. Through comprehensive fatigue testing and analysis, the effectiveness of the UHPC strengthening method is validated in terms of suppressing crack propagation and reducing stress ranges at critical details. The findings of this research confirm that the UHPC layer reinforcement can rehabilitate heavily cracked OSDs, significantly extend the fatigue life of the deck, and ensure its safe performance over the remaining service life. This study provides important experimental evidence and guidance for the use of UHPC in strengthening aging orthotropic steel bridge decks, and it offers a promising technique for extending the service life of infrastructure suffering from fatigue distress.

2 Engineering Background and Determination of Fatigue-Sensitive Details

2.1 Engineering Background

Since its opening to the public in December 2001, the Junshan Yangtze River Bridge has borne significant traffic volumes and vehicle loads, contributing greatly to the region's infrastructure with its steel box girder cable-stayed design. This iconic bridge, featuring a five-span, continuous dual-tower and dual-cable plane structure, demonstrates advanced bridge engineering techniques and serves as a vital link connecting surrounding areas. The bridge spans a total length of 2847 m with a configuration of 48 + 204 + 460 + 204 + 48 m. Its steel box girder deck uses orthotropic steel plates made of Q345C steel, which are 14 mm in thickness for its main lanes and 12 mm for its driving lanes. The bridge's pavement was designed with a double-layer SMA (Stone Mastic Asphalt) with a total thickness of 75 mm. Over time, the steel structure, particularly the orthotropic plates, has begun showing fatigue cracking due to repeated loads, posing serious challenges for traffic safety and bridge maintenance.

With increasing traffic, especially that of heavy vehicles, significant fatigue cracking emerges in structural components, such as the top plate and U-ribs, especially at connections with the diaphragms (Fig. 1). The growing number and scale of these cracks, identified during routine inspections, indicate that the current maintenance measures are inadequate. Consequently, bridge management has sought new repair and reinforcement strategies to extend the bridge's service life and ensure traffic safety.

Responding to this need, this study adopted and tested a novel decking system—a steel–UHPC composite bridge deck structure containing steel-plate strips. This system integrates a 55-mm UHPC layer connected to the deck using 13×35 mm short studs with 150-mm transverse and 200-mm longitudinal spacings. The UHPC layer's structural performance on a cracked deck was ensured by positioning an 80×8 mm transverse steel plate beneath the UHPC layer, connecting them with 13×27 mm short studs, and bonding the steel plate to the bridge steel deck with an adhesive. Compared to the traditional solution, we added transverse steel-plate strips, because the stress-sensitive locations of the steel deck are determined by its transverse bending behaviors. The traditional UHPC reinforcement scheme is not ideal as the steel bridge deck has numerous longitudinal cracks, causing discontinuity in the transverse tensile zone at the bottom of the UHPC layer, which prevents effective inhibition of further crack development. By attaching a layer of transversely arranged steel-plate strips to the cracked steel bridge deck, the steel deck becomes continuous in the transverse direction, effectively resisting the transverse

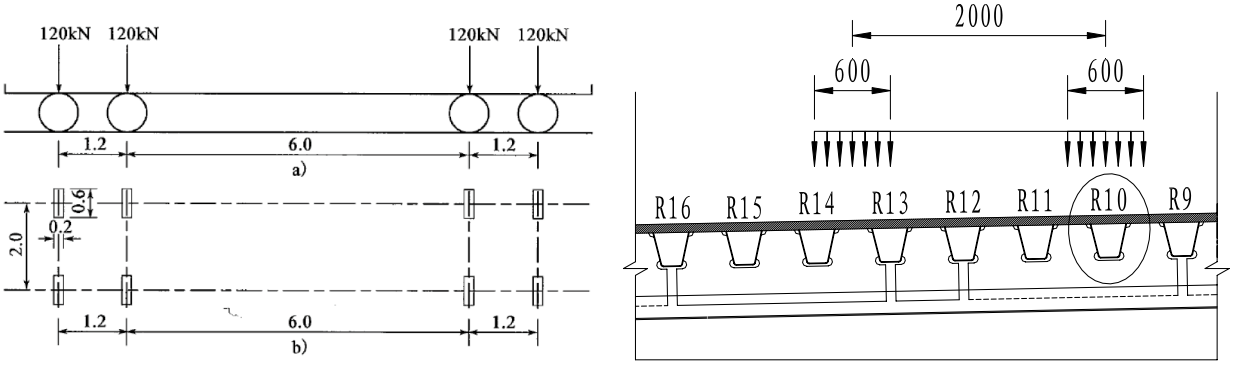

Fig. 7 Axle load of model III for fatigue analysis and axle load pattern

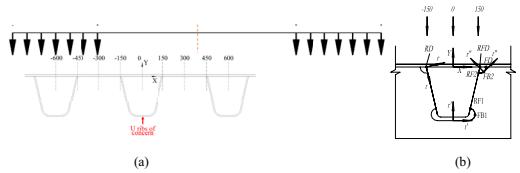

Fig. 8 Axial load transverse layout (TLWL) and local coordinate system definition

tensile stress at the bottom of the UHPC layer. This arrangement (Figs. 2 and 3) aimed to enhance the overall load-bearing capacity of the steel structure and reduce fatigue stresses without significantly increasing permanent loads. Moreover, the careful design of stud and steel-plate layouts, along with the UHPC layer's reinforcing mesh (transverse rebar diameter 12 mm, spacing 50 mm; longitudinal rebar diameter 10 mm, spacing 37.5 mm), strengthens the bridge deck's structural integrity and enhances its durability, driving comfort, and wear resistance, thereby improving the overall bridge performance.

2.2 Fatigue-Sensitive Details

The focus for the bridge's orthotropic steel deck involves fatigue details at intersections between the U-ribs and the top plate and the areas, where the diaphragms meet U-ribs and the top plate (Fig. 4a). The type of fatigue cracks at these junctions include: (1) top plate cracks originating at weld toes (C.1); (2) top plate cracks originating at weld roots (C.2); (3) U-rib wall plate cracks at weld toes (C.3); and (4) weld seam cracks originating at weld roots (C.4).

For the areas where the diaphragms, U-ribs, and the top plate intersect, the fatigue crack types (Fig. 4b, c) include: (1) cracks around diaphragm assembly holes and over weld holes (C.7 and C.7.1); (2) horizontal cracks at the top ends of lower arcuate notches in diaphragms (C.5); (3) horizontal cracks at U-rib walls above arcuate notches and over weld holes (C.6 and C.6.1); (4) vertical cracks in U-rib walls at junctions with diaphragms (C.8); and (5) top plate cracks at intersections with U-ribs and diaphragms (DPS01 and DPS01.1).

The experiment and analyses aimed to reflect the actual stress distribution and fatigue behavior around these critical details to ensure the reinforcement strategies developed were grounded in realistic structural responses to loading conditions.

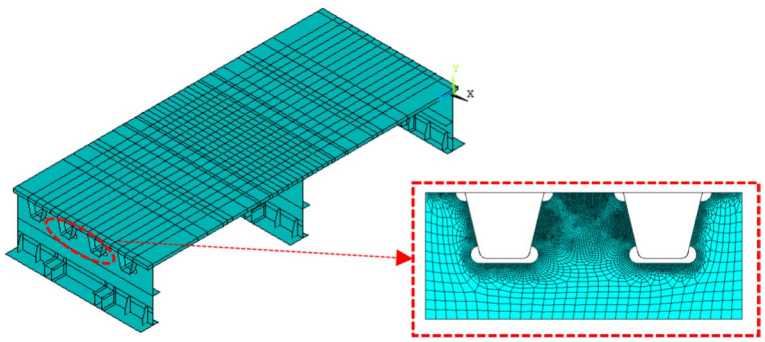

Fig. 9 Laboratory-test specimen finite-element model and partial mesh refinement schematic

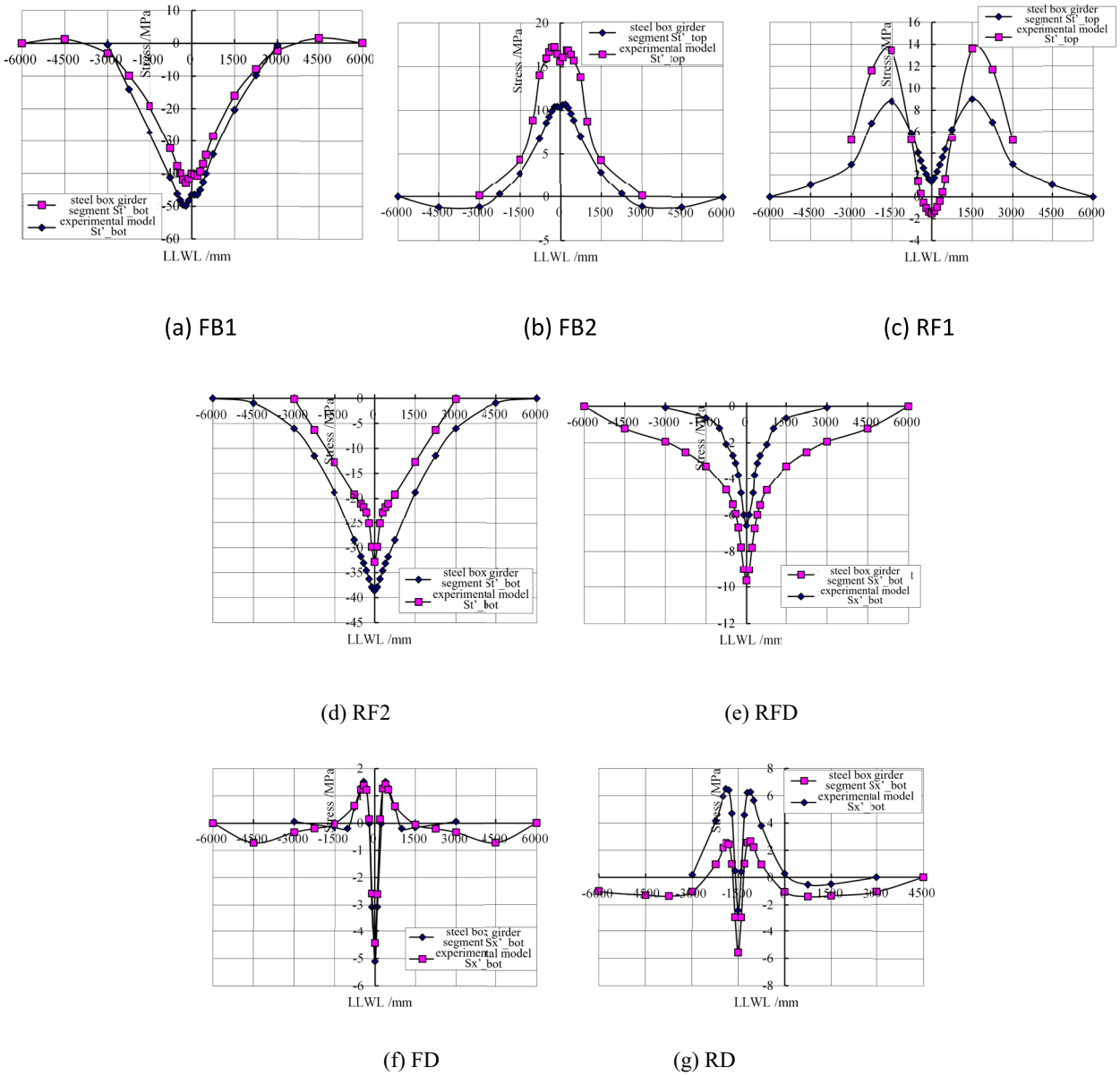

Fig. 10 Comparison of the stress influence line of every hotspot between the segment model and the laboratory-test specimen

3 Finite-Element Modeling for Laboratory-Test Specimen Design

To support the experimental program, a detailed finite-element (FE) analysis was performed as an auxiliary tool to guide the test design. Finite-element models of both the actual bridge deck segment and the laboratory-test specimen were established using ANSYS (Figs. 5 and 9). This analysis aims to show the consistency between the stress response of the laboratory-test model at key hot spots and the response value of the actual bridge segment model by comparing the stress distribution at the identified fatigue-sensitive details, which indirectly ensures the rationality of the boundary condition setting of the laboratory-test specimen.

3.1 Upgraded Steel Box Girder Segment Finite-Element Model

Along the longitudinal direction of the bridge, the upgraded steel box girder segment model consisted of a four-span structure with 5 diaphragms, with a total length of 15 m. The model's end diaphragms were those

at the locations of the stay cables, situated between the 6th and 7th cables, with the 3 middle diaphragms sequentially labeled as HGB1 to HGB3. An 8-node shell element, SHELL93, was used, with the finite-element mesh size near the concerned cross section reduced to 4 mm. The mesh partitioning was used in the local area (Fig. 5). To reduce the computational scale, the composite deck's slip action is neglected. A 55-mm solid element layer was directly established on the original steel deck using co-nodal connections; the element type was a 16-node solid element SOLID95. An elastic modulus of 52 GPa was adopted to approximate the UHPC layer. Various finite-element model boundary conditions were applied to reflect the force characteristics of the steel bridge deck in the actual structure as accurately as possible. First, symmetric constraints in the X-direction were used at the road centerline cross section. Second, at the end diaphragm cross section, the longitudinal (Z-direction) translational degrees of freedom and the rotations about the vertical (Y) and lateral (X) axes of the steel box and U-ribs were constrained to approximate the end diaphragms as internal rather than boundary support diaphragms. Third, at the end diaphragm section, the vertical (Y-direction) translational freedom of the steel box web was constrained to approximate the action of the stay cables. Based on Saint–Venant's principle, these boundary conditions ensure that the force state of the area of interest did not significantly deviate from that in the actual steel bridge deck, provided that it was sufficiently far from the model boundaries.

The analysis focused on the middle diaphragm (HGB2) and the 10th U-rib from the bridge centrelines located in the outer lane (Fig. 6).

The axle load used in this study for fatigue analysis followed the Chinese Highway Steel Structure Bridge Design Specification (JTG D64-2015) Model III. (Fig. 7), with an axle weight of 120 kN, wheelbase of 2 m, and tire footprint dimensions of 600 by 200 mm (ASHTO. AASHTO LRFD, 2012; BS EN 1993-1-9:2005 Eurocode 3: Design of steel structures 2005; EN 1993-2:2006 Eurocode 3: Design of steel structures 2006; Japanese Road Association, 2012). In the finite-element analysis, the load was applied through influence surfaces to obtain the stress influence surfaces for the primary fatigue-sensitive parts to determine the effects of fatigue truck loading. Specifically, in the transverse direction, the wheel center of the axle load was positioned relative to the concerned U-rib (Fig. 8a), covering positions TLWL = −600, −450, …, 0, …, 450, 600 mm.

For convenience, the local coordinate systems used in the analysis (Fig. 8b) were as follows:

1. X–Y Cartesian coordinate system, with the origin at the center of the U-rib, to describe the stress state of the deck plate;
2. t–r curved coordinate system, with the origin at the center of the bottom of the U-rib, to describe the stress state of the U-rib;
3. t'–r' curved coordinate system, with the origin at the center of the bottom of the arc cut at the diaphragm assembly hole, to describe the stress state at the diaphragm assembly hole;

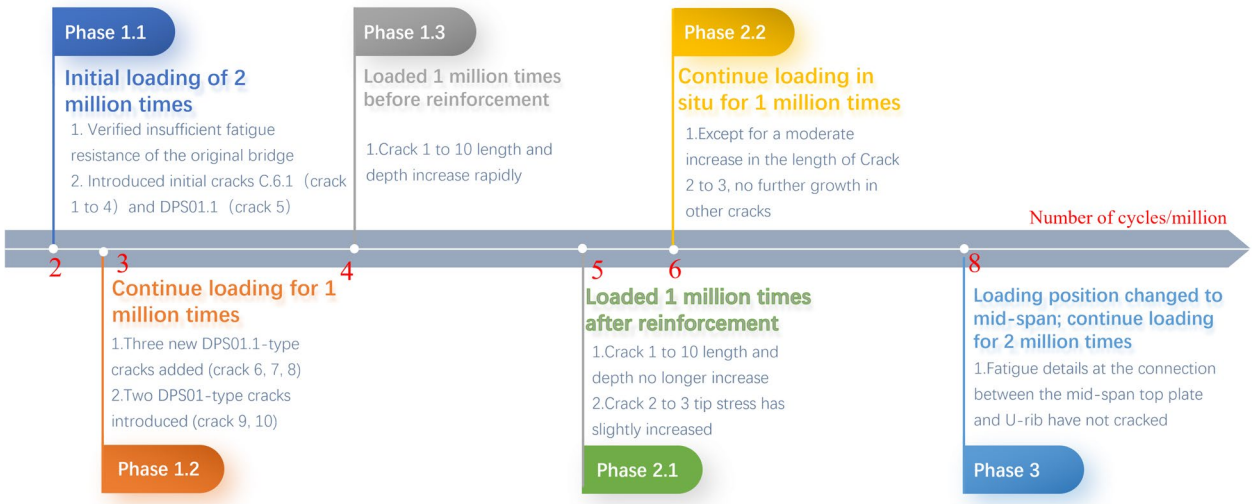

Fig. 11 Loading process axis diagram of the laboratory-test specimen

4. t"–r" curved coordinate system, with the origin at the bottom of the cut-out at the diaphragm pass hole, to describe the stress state at the diaphragm pass hole.

3.2 Finite-Element Model of the Laboratory-Test Specimen

The laboratory-test specimen's finite-element analysis involved 8-node shell elements (SHELL93) for steel structures and 16-node solid elements (SOLID95) for the UHPC layer (Fig. 9). The analysis focused on the middle diaphragm (the second diaphragm) and the middle two U-ribs. The boundary conditions of the Laboratory-Test Specimen are as follows: at the bottom edges of the three transverse diaphragms, the longitudinal (Z-direction) translational degrees of freedom and the rotations about the vertical (Y) and lateral (X) axes are constrained. The loading also followed the fatigue load model III specified in the Chinese specification; it was applied through the influence surfaces without considering the load distribution action of the deck pavement layer. In the transverse direction, the wheel load was placed at the center of the 2 middle U-ribs (Fig. 7). Longitudinally and relative to the concerned middle diaphragm, the wheel load could move to positions, including LLWL = −3000, −1500, …, 0, …, 1500, 3000 mm; LLWL = −3000, 0, and 3000 mm corresponded to the positions of the first, second, and third diaphragms, respectively.

3.3 Consistency Analysis of Laboratory-Test Specimen and Steel Box Girder Segment Model

Figure 10a–g, respectively, presents the stress influence lines at hotspots FB1 (Diaphragm Assembly Hole Hotspot), FB2 (Diaphragm Pass-Hole Hotspot), RF1 (U-Rib and Diaphragm Assembly Hole End Hotspot), RF2 (U-Rib and Diaphragm Pass-Hole End Hotspot), RFD (Intersection Hotspot of U-Rib, Diaphragm, and Deck Plate), FD (Deck Plate and Diaphragm Pass-Hole End Hotspot), and RD (Mid-span Hotspot at the Deck Plate and U-Rib Connection) in both the retrofitted steel box

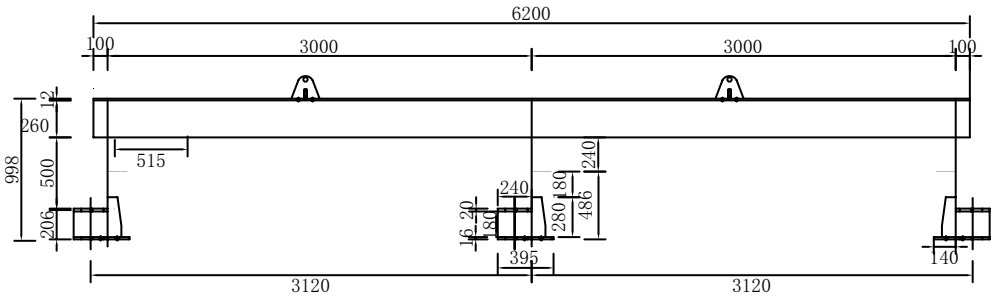

(a) Elevation drawing.

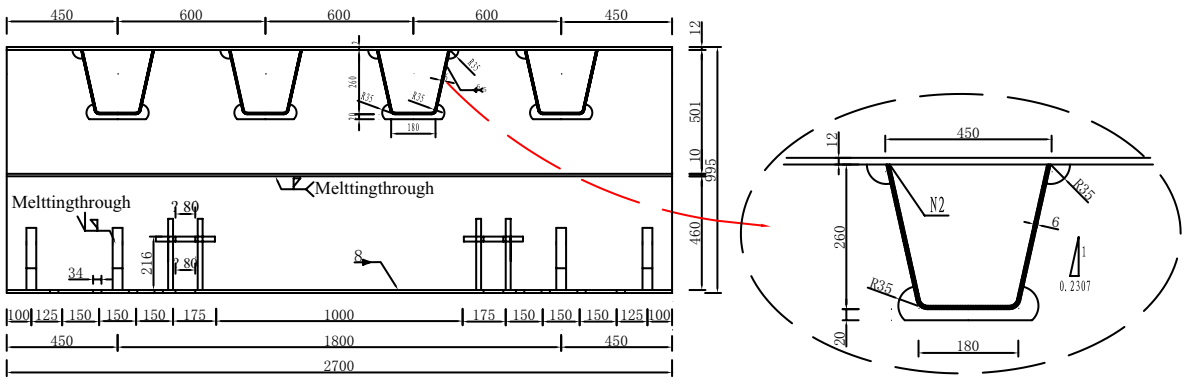

(b) Diaphragm cross-section. (c) Large sample size of U-rib and diaphragm arcuate notch.

Fig. 12 Preliminary laboratory-test specimen scheme before composite bridge deck reinforcement

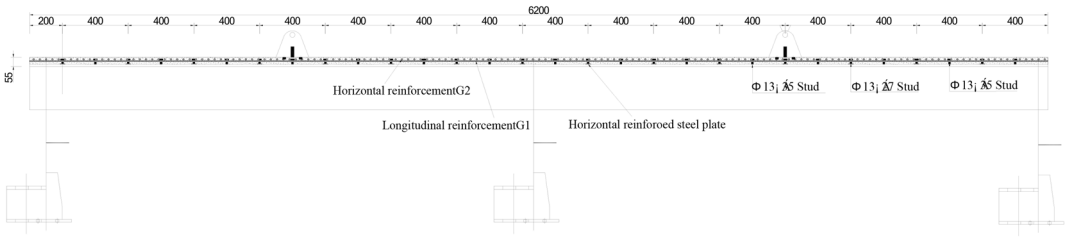

(a) Elevation drawing.

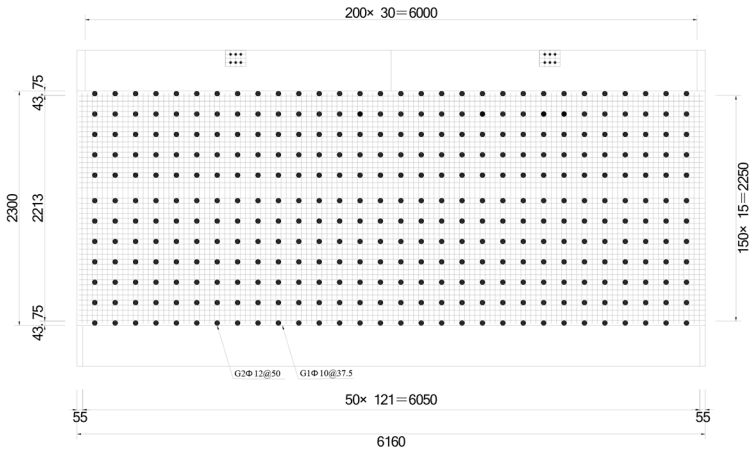

(b) Plan view.

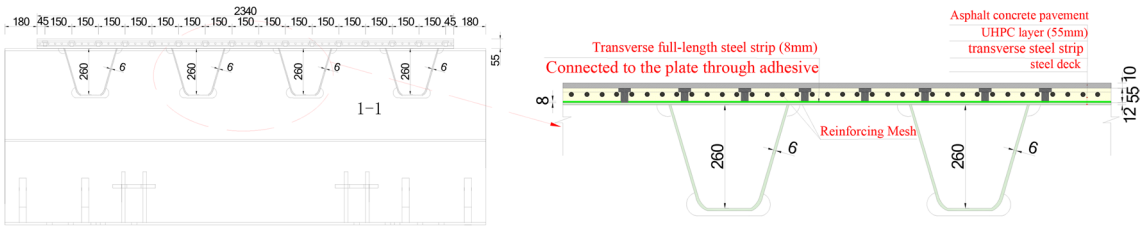

(c) Diaphragm cross-section.

(d) Large sample of the steel-UHPC layer.

Fig. 13 Scheme of laboratory-test specimen of composite bridge deck

girder model and the Laboratory-Test Specimen when TLWL = 0 and as the wheel load moves longitudinally along the bridge. For hotspots FB1, FB2, RF1, and RF2, the controlling stress (maximum principal stress) is generally the maximum shear stress St at that point. For hotspots RFD, FD, and RD, the controlling stress is generally the normal stress Sx at that point. Here, 'top' is used to indicate the + Z-direction side of the plate, where the hotspot is located, and 'bot' represents the -Z-direction side of the plate. For example, St'_top represents the maximum shear stress on the + Z-direction side of the plate at the hotspot, and Sx'_bot represents the maximum normal stress on the -Z-direction side of the plate at the hotspot.

From Fig. 10, it can be seen that the shape and magnitude of the stress influence lines at various hotspots in both the retrofitted steel box girder segment model and the Laboratory-Test Specimen show good consistency. In addition, from the stress influence line at hotspot RFD, it can be observed that the maximum stress amplitude

Table 1 Material characteristics and test methods

Material	Nominal grade/specification	Verified property values	Test standard/method
Deck-plate & U-rib steel	Q345C (GB/T 700)	fy = 358 MPa, E = 206 GPa	Tensile coupon tests, GB/T 228.1-2021
Diaphragm steel	Q345C	fy = 355 MPa, E = 205 GPa	same as above
Transverse steel–plate strips	Q345C	same as deck steel	–
Stud shear connectors	Φ13 × 35 mm, Q345	Visual bend test + hardness check	GB/T 10433-2002
Rebar in UHPC mesh	HRB400 (Φ10, Φ12)	fy = 437 MPa, E = 200 GPa	Tensile test, GB/T 228.1-2021
UHPC (28 days)	In-house mix, w/b = 0.18, 2 vol% 13 mm brass-coated steel fibers	fc,28 = 151 MPa (cube), ft,28 = 8.2 MPa (direct tension), E = 52 GPa ρ = 2.55 t m^{-3}	GB/T 50081-2019 (compression & modulus), JSCE-SF4 (direct tension)

(a) CNC blanking. (b) Spot welding and grinding of the top plate and U-ribs. (c) Diaphragm unit fabrication. (d) Welding forming.

Fig. 14 Main manufacturing process of the laboratory-test specimen pieces

in the segment model at this hotspot is 10 MPa. When compared with the health monitoring data of the in-situ measurements on a real bridge provided later (Fig. 32), it is found that the stress amplitude obtained from finite-element simulation at hotspot RFD is almost identical to the measured stress amplitude at this location (9.9 MPa). Therefore, the stress response of the laboratory-test specimens designed in this study can effectively represent the actual bridge and is suitable for conducting fatigue tests.

4 Experimental Implementation and Results Analysis

4.1 Test Method (Three-Phase Fatigue Loading Program)

The experimental program was carried out in three successive phases of fatigue loading, designed to evaluate the deck's performance before reinforcement, after reinforcement, and under extended service loading. As shown in Fig. 11, to assist readers in understanding, a loading process axis diagram is drawn.

In Phase 1, the as-built steel orthotropic deck specimen (without UHPC) was subjected to focused cyclic loading at a critical diaphragm region to initiate fatigue cracks in the known vulnerable details. A total of 3 million load cycles were applied at the transverse diaphragm (support) location of the deck to reproduce damage equivalent to long-term service and to induce fatigue cracking at the typical hotspot details (such as the rib-to-deck welds and cut-out details around the diaphragm). Immediately following this, an additional 1 million cycles were applied at the same location (with the same loading configuration) to monitor the progression of the initial cracks. This extended loading ensured that cracks grew to measurable lengths, thereby simulating a severely cracked deck condition prior to any repair. By the end of Phase 1 (total 4 million cycles), the inadequate of fatigue resistance of the unreinforced orthotropic deck was confirmed when multiple fatigue cracks had formed and propagated in the expected critical areas of the steel deck.

For Phase 2, the test specimen was retrofitted with the proposed reinforcement and then re-tested to assess the improvement in fatigue performance. The reinforcement involved attaching steel-plate strips over the rib-to-deck weld seams and casting a UHPC layer (55 mm thick) on top of the steel deck, transforming it into a steel–UHPC composite deck. After the retrofit was completed and properly cured, the specimen was again subjected to cyclic loading at the same diaphragm location for 1 million cycles. This post-reinforcement loading used the same load amplitude and setup as Phase 1, allowing a direct comparison of crack growth

(a) Marking and welding studs (b) Transverse steel strip welding studs (c) Applying transverse steel strips (d) Binding rein forcement

Fig. 15 Construction stage before UHPC casting

rates and stress responses before and after reinforcement. If a significant slowdown or even stagnation of the existing crack propagation is observed during this phase of testing, it will prove the positive effect of the UHPC layer and steel slats in improving the fatigue resistance of the bridge deck.

In Phase 3, a final extended fatigue test was conducted to verify the long-term durability of the reinforced deck under service-like conditions. In this phase, the loading location was shifted to simulate a vehicle traveling over the span: a two-point cyclic loading was applied at the mid-span region of the deck specimen. Two hydraulic actuators were used simultaneously, positioned underneath the deck to apply loads through the second and third U-ribs (R2 and R3) at mid-span. The actuators were driven in an asynchronous phase (out-of-phase by 90°) to simulate dual-wheel truck loading moving across the span, with a peak-to-peak load range of 30kN to 230kN on each actuator. The phase difference caused the load peaks to occur alternately, creating a dynamic effect representative of moving wheel loads. The reinforced deck specimen was subjected to 2 million cycles of this dual-point loading at mid-span. This final prolonged loading phase was equivalent to the deck experiencing many years of service after reinforcement. By the end of Phase 3, the specimen underwent approximately 8 million load cycles in total. This three-stage fatigue loading program provided a comprehensive assessment: Phase 1 verified the deck's vulnerability and induced cracks, Phase 2 demonstrated the immediate effect of the reinforcement, and Phase 3 confirmed the fatigue durability of the reinforced deck throughout its designed service life.

4.2 Test Specimen Dimensions and Fabrication

The test specimen was a full-scale orthotropic steel deck segment fabricated to replicate the actual bridge deck details of the Junshan Yangtze River Bridge. A longitudinal two-span structure of 3.0 + 3.0 m was selected, cutting across 4 U-ribs, with the top plate thickness at 12 mm, U-rib thickness at 6 mm, and diaphragm web at 8 mm (Fig. 12). These dimensions and the arcuate notches match the real bridge's specifications. The composite deck retrofit involved attaching studs and steel strips to the top plate and casting a 55-mm UHPC layer, forming the steel–UHPC composite structure (Fig. 13). All diaphragms were anchored using bolts or screws.

The material property values of each component of the specimen and the test method are shown in Table 1

Fabrication of the steel deck specimen was carried out by a professional bridge fabrication company in strict accordance with standard bridge manufacturing procedures. Figures 14 and 15 illustrate the key fabrication steps; Fig. 16 records UHPC casting and curing. All welding procedures, consumables, and inspection criteria match those specified for the actual bridge, ensuring that fatigue-sensitive weld details in the test model behave identically to those in service. No artificial notches were introduced; cracks were allowed to initiate naturally during Phase 1 loading.

4.3 Loading Setup and Measurement Techniques

All fatigue loading in the experiments was applied using computer-controlled servo-hydraulic actuators mounted on a strong floor reaction frame. The steel–UHPC deck specimen was simply supported at its ends on robust supports that allowed vertical reactions while permitting slight rotations (simulating pin supports). Additional restraint frames were used as needed to emulate the effect of continuity with adjacent spans, as guided by the FE analysis (this ensured the specimen's boundary conditions mimicked an interior span of the bridge). In Phase 1 and Phase 2, a single hydraulic actuator was positioned above the transverse diaphragm location of interest (Fig. 17a). The actuator applied a cyclic load through a stiff loading beam that distributed the force to the deck surface over a patch approximating a truck tire contact area. The load was cycled between a minimum of 30kN and a maximum of 230kN at a frequency selected to avoid resonance (approximately 2–3 Hz, ensuring millions of cycles could be applied in a reasonable time).

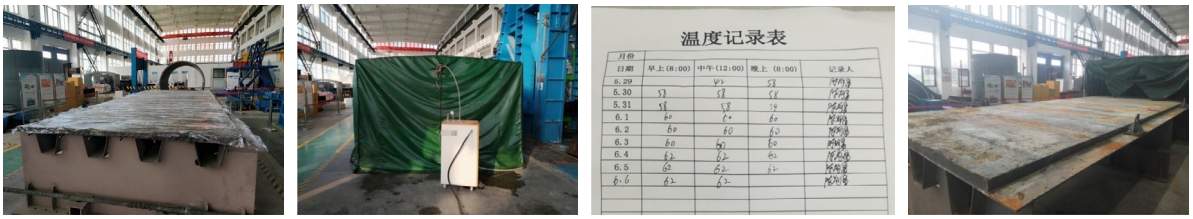

(a) Film covering wet curing. (b) Steam curing shed. (c) Steam curing record. (d) Final formed test piece.

Fig. 16 Curing stage of the composite bridge deck test piece

This loading range corresponded to the effect of a heavy truck wheel passing over the diaphragm region, producing significant stress ranges at the nearby welded details. In Phase 3, the loading setup was modified to incorporate two actuators for the two-point loading at mid-span, as shown in Fig. 17b. The two actuators were synchronized with a 90° phase lag: when one actuator was at its peak load (230 kN), the other was at its minimum (30 kN), and vice versa. This created an alternating pulsating load pattern that simulated a moving pair of wheel loads traversing the span. Both actuators in Phase 3 were operated with the same peak-to-peak amplitude (30–230 kN) and frequency, and their loading heads were placed above the top of the UHPC layer in alignment with the second and third U-ribs from the deck edge. The out-of-phase two-point loading induced a realistic flexural response in the span and caused the critical diaphragm and mid-span regions to experience concurrent cyclic stresses, thereby testing the deck's fatigue performance under a complex loading scenario. Over the course of Phase 3's 2 million cycles, the actuators maintained stable load control, and no unexpected load drops or interruptions occurred.

Throughout all phases of testing, a comprehensive instrumentation and measurement plan was implemented to monitor the structural response and detect crack developments, as shown in Fig. 18. A network of strain gauges was installed at critical locations on the steel deck and the UHPC surface. For the steel deck, strain gauges were placed on the bottom side of the deck plate directly under the troughs of several U-ribs (DBT series gauges) and on the top surface of the deck plate (DDT series) near expected crack sites, to record the local strain ranges during loading. Additional gauges were attached to the vertical sides of the U-ribs (RV series gauges, oriented vertically) and along the longitudinal direction on the U-ribs (RL series) to measure rib deformation. Strain rosettes were also arranged around the cut-out corners of transverse diaphragms (CB series gauges) to capture the strain concentration at those geometrically discontinuous details. For the UHPC layer, strain sensors on the surface were arranged both transversely and longitudinally to measure the composite action with the steel deck. In total, during the initial diaphragm loading phases (Phase 1 and 2), on the order of several dozen strain measurement points were monitored, covering all key components (deck plate, ribs, and diaphragm joints). In the final phase (Phase 3), the instrumentation layout was slightly adjusted: some gauges on the UHPC top surface were reoriented to the longitudinal direction to better capture mid-span bending strains, and additional gauges were installed at mid-span regions of interest, resulting in a total of 19 active strain gauges during Phase 3.

In addition to strains, displacement transducers were used to measure deflections of the deck. Four displacement sensors were positioned at representative mid-span points (e.g., under the actuators and at mid-span between actuators) and near the loaded diaphragm to track the vertical displacements under cyclic loading. These measurements helped ensure the applied loading remained within elastic range (aside from localized crack deformation) and provided data on any stiffness changes in the deck as cracks formed or as the UHPC layer took effect. The load input from the actuators was continuously recorded by the control system, and the history of applied cycles was logged to verify the number of cycles and load range.

Table 2 summarizes the distribution of all instrumentation used during the three experimental phases. In Phase 1 (pre-retrofit), 33 strain gauges were installed to capture the global response of the unreinforced deck: five groups covered the deck plate (DBT and DDT series), the U-rib web (RV and RL), and the diaphragm junctions (CB), thereby mapping both in-plane and out-of-plane strains around the most fatigue-sensitive details. Phase 2 (immediately after retrofit) focused on tracking crack-tip behavior, so eight additional gauges were bonded directly at the U-rib wall (LFU) and deck-plate crack tips (LFD), while four transverse gauges (DT) were embedded on the UHPC surface to monitor composite action; the

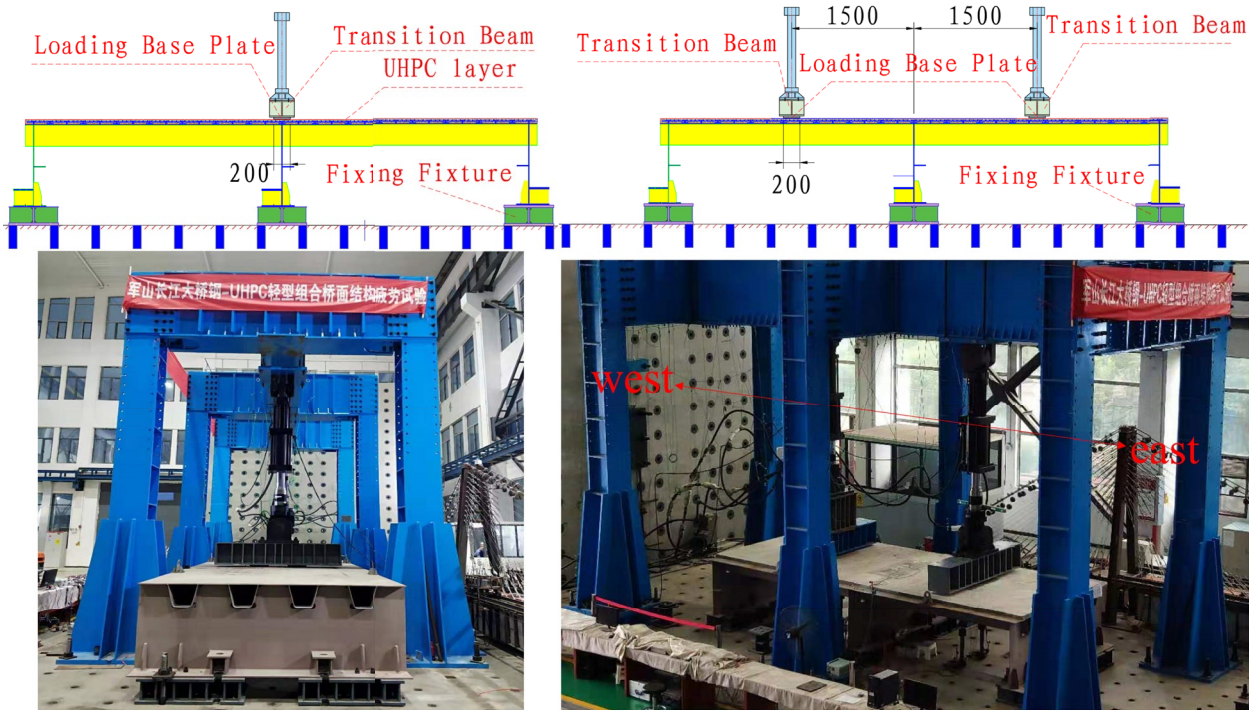

(a) in phase 1 and phase 2 (b) in phase 3

Fig. 17 Schematic diagram of specimen placement and loading position

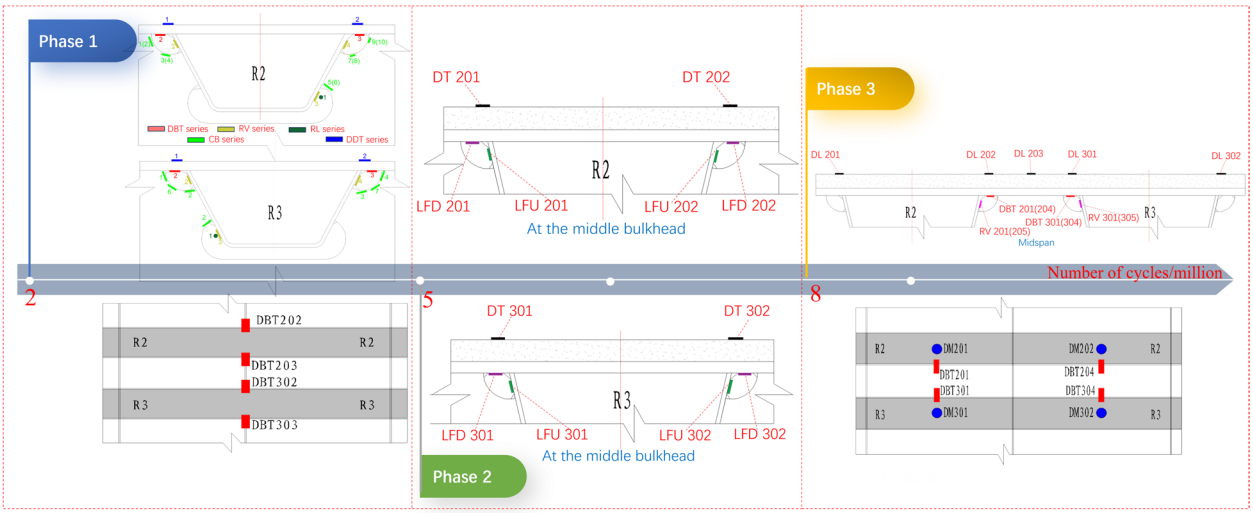

Fig. 18 Strain gauge and displacement gauge layout at each loading stage

total instrumentation count in this phase was 41. For the long-term Phase 3 test, the layout was refined to observe mid-span bending of the strengthened deck: a fresh set of DBT and RV gauges recorded steel strains, five longitudinal DT gauges measured UHPC surface strains, and four displacement transducers (DM series) captured vertical deflection of the U-rib mid-span. Altogether, the program employed twelve instrument families—11 for strain and one for displacement—providing a comprehensive, phase-specific picture of how the deck and the

new UHPC layer shared load and evolved under eight million fatigue cycles.

Data acquisition was conducted at regular intervals to observe the evolution of the deck's response. Rather than recording continuously (which would generate an immense data volume for millions of cycles), the system was configured to record a set of readings every 250,000 cycles. At these intervals, the test was briefly paused and a full set of static and dynamic measurements was taken: the current crack lengths were measured by visual inspection and crack gauges, strain gauge readings under a reference load were recorded, and any changes in structural stiffness were inferred from displacement measurements. This interval-based monitoring allowed tracking of fatigue crack initiation and propagation over time. For example, after each block of 0.25 million cycles in Phase 1, the crack lengths at the rib-to-deck welds were measured to see how quickly they grew; similarly, the strain range at gauges near those cracks was checked for increases that would indicate a loss of cross-sectional area or stiffness. In Phase 2 and Phase 3, the same periodic checks were performed to compare the behavior pre- and post-reinforcement. The measurement data confirmed that after the UHPC layer was added, the strain ranges at formerly critical locations dropped significantly (for instance, the nominal strain-derived stress amplitude at a crack tip reduced from ~ 75 MPa before retrofit to ~ 10 MPa after retrofit), reflecting the improved fatigue performance. Throughout Phase 3, the strain and deflection readings remained stable, and no new cracks were observed, indicating that the reinforced deck maintained its integrity under the extended loading.

In summary, the experimental setup and instrumentation were carefully designed to capture the essential responses of the orthotropic steel–UHPC composite deck under fatigue loading. The three-phase loading regime, combined with detailed measurements, provided a full picture of the deck's fatigue behavior: from crack initiation in the unreinforced state to performance after reinforcement and finally the durability under prolonged cyclic loading.

4.4 Laboratory-Test Specimen's Results and Analysis at Each Stage

4.4.1 Fatigue Mechanism and Evaluation Criteria

The tested orthotropic steel deck is governed by high-cycle fatigue under nominal stress ranges of 40–90 MPa and a stress ratio $R = P_{min}/P_{max} \approx 0.13$. Weld-toe cracking initiates at the deck-to-rib fillet (detail C.6.1) and the diaphragm pass-hole (detail DPS01.1) due to a combination of (i) out-of-plane distortion between rib and diaphragm, and (ii) local bending of the deck plate.

Crack initiation is detected when the measured stress range at a control gauge falls by > 20%, indicating loss of stiffness in the local load path. Crack propagation is tracked by periodic crack-length measurement. For comparison with design limits, the experimental S–N data are plotted against the Eurocode EN 1993-1-9 FAT curves (FAT 90, FAT 125, FAT 160), which represent constant-amplitude fatigue strength at 2×10^6 cycles for similar weld geometries. Failure is defined as:

a through-thickness crack penetrating the rib wall (C.6.1) or.

a surface crack exceeding 7.5 mm depth in the deck plate (DPS01.1).

Table 2 Classification and statistics of measurement points

Phases	Serial No	Code	Code location description	Count	Category
1	1	DBT Series	Transversely arranged at the bottom surface of the top plate	4	Strain Measurement Points
	2	RV Series	Vertically arranged on the side of the U-rib	6	
	3	RL Series	Longitudinally arranged on the side of the U-rib	2	
	4	CB Series	Around transverse diaphragms intersecting with U-ribs	17	
	5	DDT Series	Transversely arranged at the top surface of the top plate	4	
2	6	LFU Series	U-rib Wall Plate Crack Tip	4	
	7	LFD Series	Crack Tip at the Bottom Surface of the Top Plate	4	
	8	DT Series	Strain Gauge Long Edge Placed Transversely on the Top Surface of the UHPC Layer	4	
3	9	DBT Series	Transversely arranged at the bottom surface of the top plate	4	
	10	RV Series	Vertically arranged on the side of the U-rib	4	
	11	DT Series	Strain Gauge Long Edge Placed Longitudinally on the Top Surface of the UHPC Layer	5	
	12	DM Series	Bottom Surface of U-Rib at Mid-span	4	Displacement Measurement Point

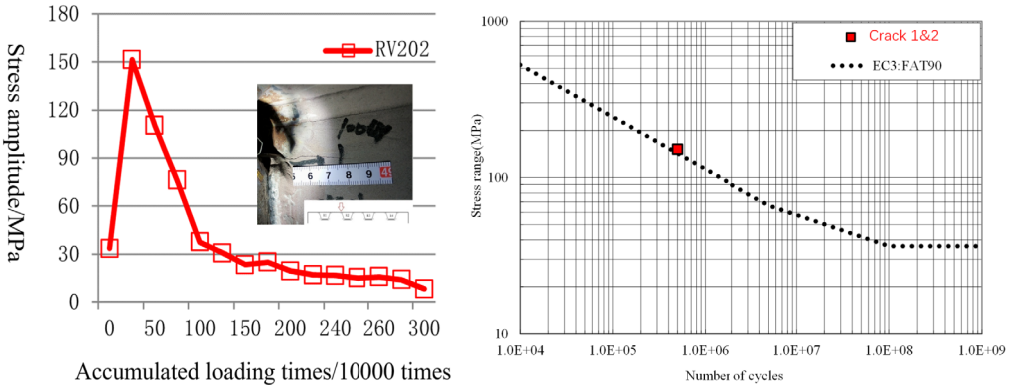

(a) crack 1&2

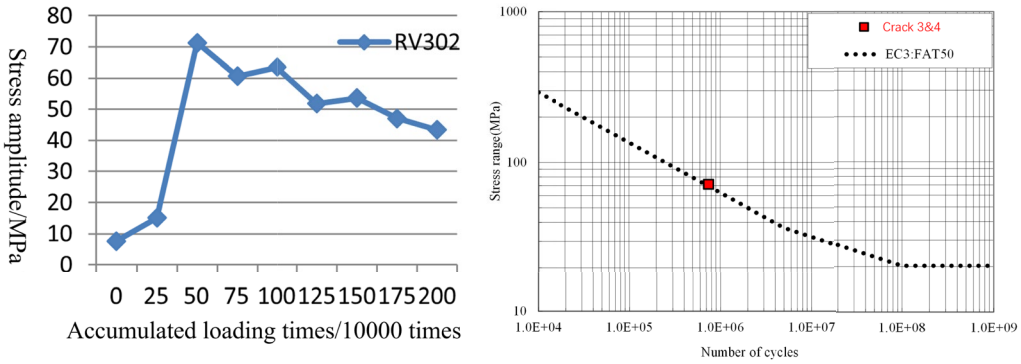

(b) crack 3&4

Fig. 19 Stress changes at the measuring point near the initial fatigue crack and the corresponding fatigue strength curve

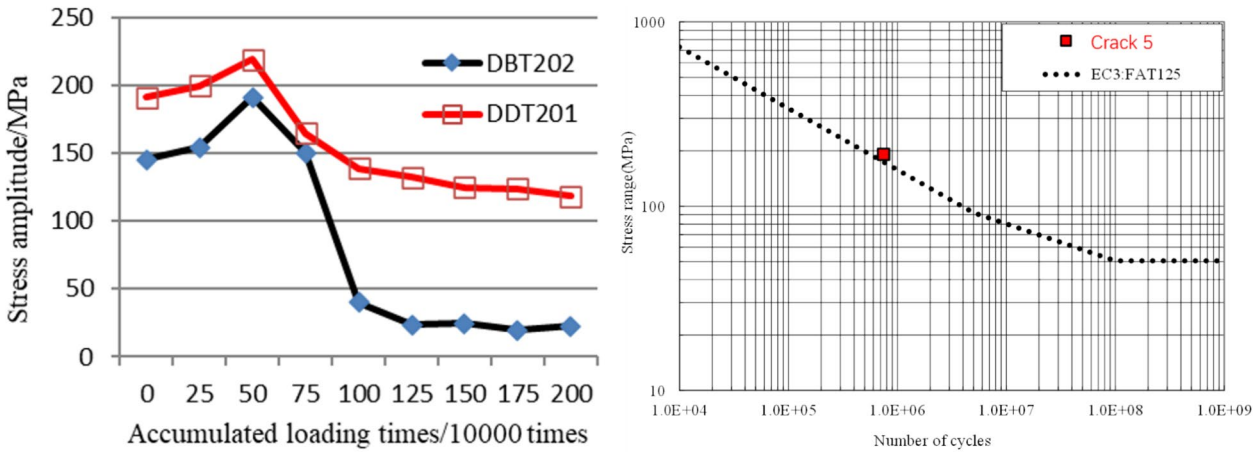

Fig. 20 Stress changes at the measuring point near fatigue crack 5 and its fatigue strength curve

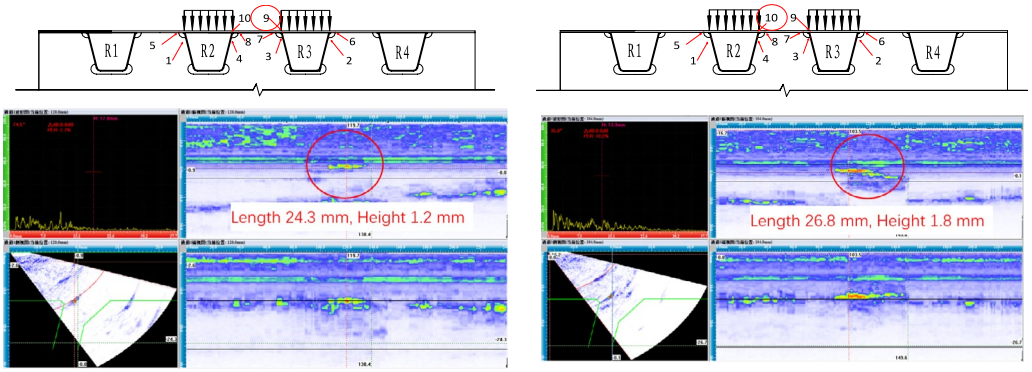

(a) crack 9/DPS01 (b) crack 10/DPS01

Fig. 21 Non-destructive inspection results for DPS01 fatigue cracks at 3 million cycles

4.4.2 Fatigue Resistance Validation and Crack Induction Phase

During the first phase of fatigue testing, fatigue cracks were detected in key stress-sensitive areas, primarily categorized as C.6.1 and DPS01.1/DPS01 types.

Figure 19a plots the stress-range–cycle (S–N) curve for *Crack 1* and *Crack 2* together with the reference FAT90 design line. When the number of cycles reached 5×10^5, the stress range recorded at gauge RV202 had fallen by 27.2%, marking the initiation of Cracks 1 and 2 at the weld ends between ribs R2/R3 and the diaphragm pass-hole.

Figure 19b presents the corresponding S–N curves for *Crack 3* and *Crack 4* (same welded detail, different gauge position) against the same FAT90 benchmark. At 7.5×10^5 cycles the stress range at gauge RV302 had decreased by an additional 15.1%, and Cracks 3 and 4 were visually confirmed.

In both sub-figures, the experimental S–N trajectories lie well above the FAT90 line in the high-cycle domain, demonstrating that the C.6.1 weld detail is highly fatigue-sensitive under the applied loading regime.

During Phase 1, fatigue cracks of the DPS01.1 detail were also detected.

As illustrated in Fig. 20—which plots the stress-range-cycle (S–N) trajectory of Crack 5 against the Eurocode FAT90 design curve—the stress ranges recorded at gauges DBT202 and DDT201 dropped by 21.2% and 24.8%, respectively, at 7.5×10^5 cycles, signaling crack initiation at the diaphragm bottom.

With continued loading, the S–N curve in Fig. 20 shows three additional drops. Between 2.4×10^6 and 2.8×10^6 cycles, Cracks 6, 7, and 8 were confirmed, each accompanied by a pronounced reduction in stress range at nearby gauges. Although only the FAT90 benchmark is plotted, the measured stress levels at these later stages fall well above the Eurocode FAT125 and approach the FAT160 domains, underscoring that the DPS01.1 detail offers insufficient fatigue resistance within the bridge's design life. These observations corroborate the vulnerability of the diaphragm-to-deck weld region under prolonged high-cycle loading.

DPS01-type fatigue cracks were detected internally using non-destructive ultrasonic testing: after 3 million cycles, Cracks 9 and 10 were identified within the deck plate (Fig. 21). These cracks penetrated up to 15% of the deck-plate thickness, with maximum depths of 1.8 mm. Despite not immediately reaching critical levels requiring repair, their existence indicates that internal deck-plate details are also at significant risk under prolonged fatigue loading.

In summary, by the end of the cumulative fatigue loading of 2 million cycles, a total of five fatigue cracks had developed. During this period, these cracks were regularly monitored, and it was found that the lengths of all existing fatigue cracks continued to extend. Cracks 1–4 had fully penetrated the U-rib wall plate (6 mm in thickness). This confirmed the inadequate fatigue resistance of the typical fatigue-sensitive detail C.6.1 on the U-rib wall plate and the DSP01.1 detail on the top plate within the bridge's design life.

After a total of 3 million loading cycles, a total of ten cracks were introduced. The length progression of each crack (excluding internal Cracks 9 and 10) is shown in Fig. 22. The overall status of the cracks during this phase is summarized in Table 3.

In Table 3, the four C.6.1 weld-toe cracks (Cracks 1–4) dominated the damage scenario: each initiated before 0.75 million cycles and, by the three-million-cycle mark, had penetrated the entire 6 mm rib wall while reaching lengths of 112–149 mm. In contrast, diaphragm-corner

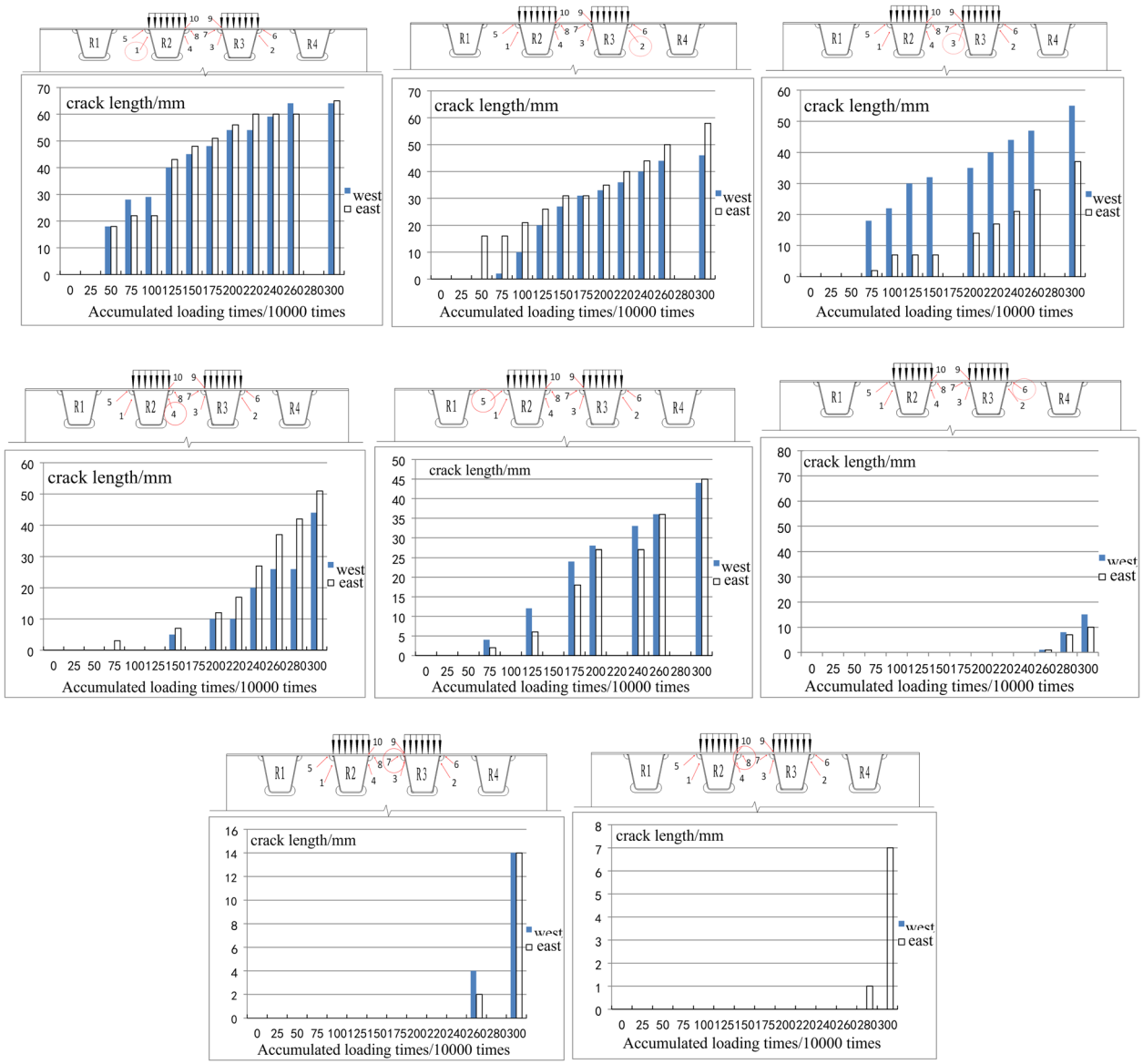

Fig. 22 Periodic inspection results of cracks after 3 million cycles of loading

cracks of type DPS01.1 (Cracks 5–8) appeared later and progressed more slowly, achieving lengths of only 27–109 mm and depths below one-quarter of the 12 mm deck-plate thickness. Sub-surface root cracks classified as DPS01 (Cracks 9 and 10) were detected ultrasonically but remained short (≈ 25 mm) and shallow (≈ 1–2 mm). These data confirm that, under the applied loading regime, the rib-to-deck weld (detail C.6.1) is the critical fatigue hotspot, whereas deck-plate cracks develop later and at a slower rate.

4.4.3 Pre- and Post-reinforcement Fatigue Loading Phase

During the first million cycles of pre-reinforcement fatigue loading (of a total of 3–4 million cycles), observation of crack propagation around the R2 rib revealed further deterioration of cracks 1 and 8 after an additional 20 million cycles (a total of 3.2 million cycles) and crack 4 after an additional 40 million cycles (a total of 3.4 million cycles) (Fig. 23). Furthermore, a Youlian Digital Ultrasonic Flaw Detector PXUT-320C was used to examine the length and depth progression of the cracks around the top plate near the R2 rib. The inspection results are shown in Fig. 24. The figure reveals that both the length

Table 3 Summary of fatigue cracks introduced after 3 million cycles

Crack number	Crack type	Cumulative load cycles at initiation/10000	Length at 3 million cycles (mm)	Depth at 3 million cycles (mm)
1	C.6.1	50	149*	6 (through)
2	C.6.1	75	124*	6 (through)
3	C.6.1	75	112*	6 (through)
4	C.6.1	75	115*	6 (through)
5	DPS01.1	75	109*	2.5#
6	DPS01.1	250	45*	1.9#
7	DPS01.1	240	48*	1.5#
8	DPS01.1	280	27*	0.9#
9	DPS01	–	24.3#	1.2#
10	DPS01	–	26.8#	1.8#

* The crack length is the sum of the extension lengths on both sides + the thickness of the partition (8 mm) + the size of the weld toe (6 mm) × 2. 2). #Ultrasound examination results. 3). – indicates no significant changes or unavailability

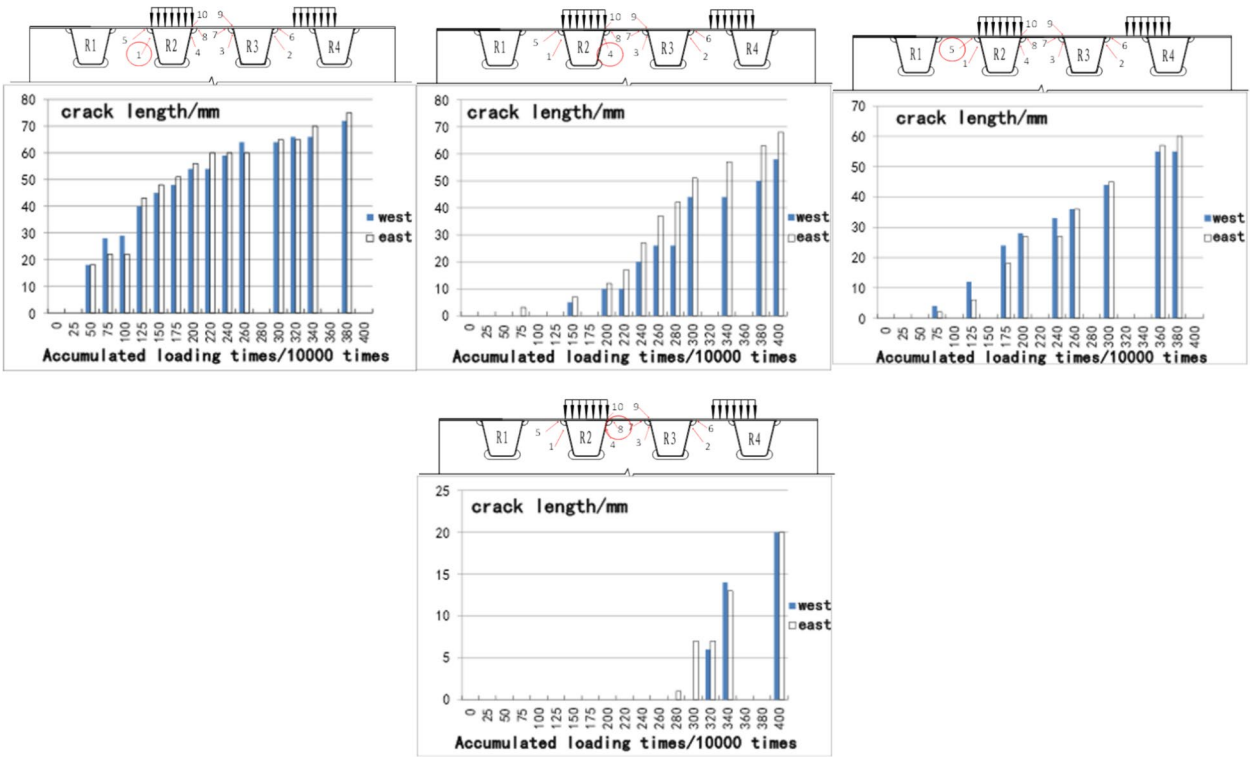

Fig. 23 Results of visible crack changes around the R2 rib before deck reinforcement

and penetration depth of the existing cracks in the top plate have continued to deteriorate and increase. Specifically, the penetration depth of Crack 5 has reached 7.8 mm, approximately 65% of the top plate thickness, and the crack length has grown from 109 to 135 mm, surpassing the threshold for repair as outlined in the top plate crack maintenance directive. In summary, before the composite bridge deck retrofit, all existing cracks exhibited rapid and significant deterioration with the accumulation of load cycles.

Post-reinforcement observations (from 4 to 5 million cycles) indicated no visible changes in crack lengths around R2 and R3 ribs, and stress amplitudes at the crack tips did not show significant variation, except for an increase at the tip of Crack 2 on the R3 rib wall (Fig. 25). Despite the increase in stress at the tips of these

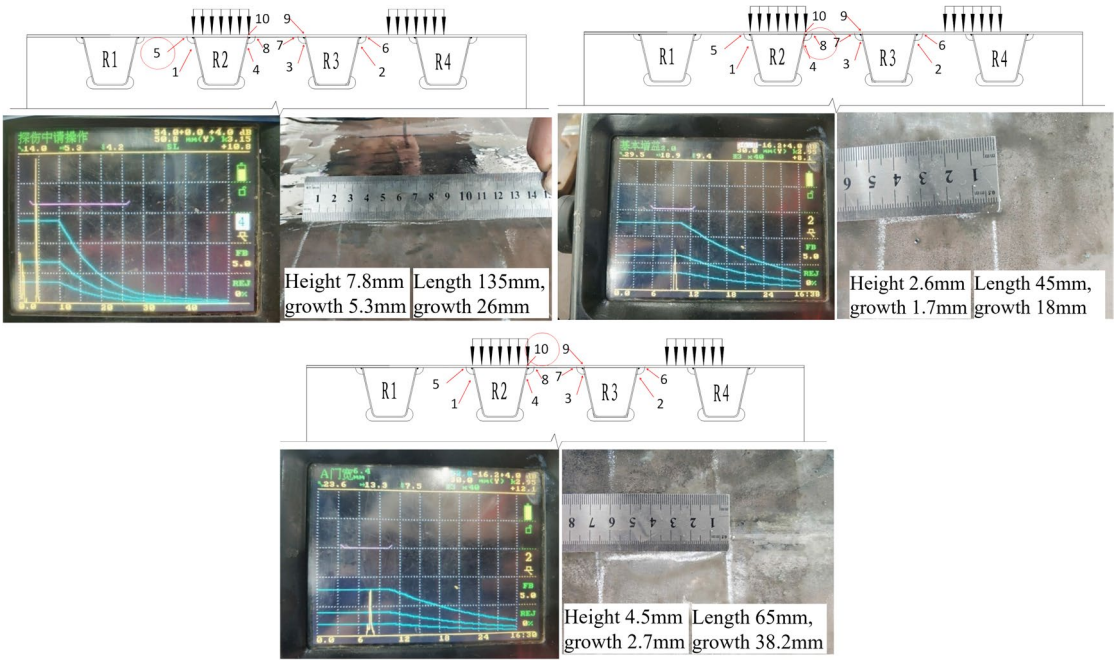

Fig. 24 Inspection results of internal cracks around the top plate near R2 rib before composite deck retrofit

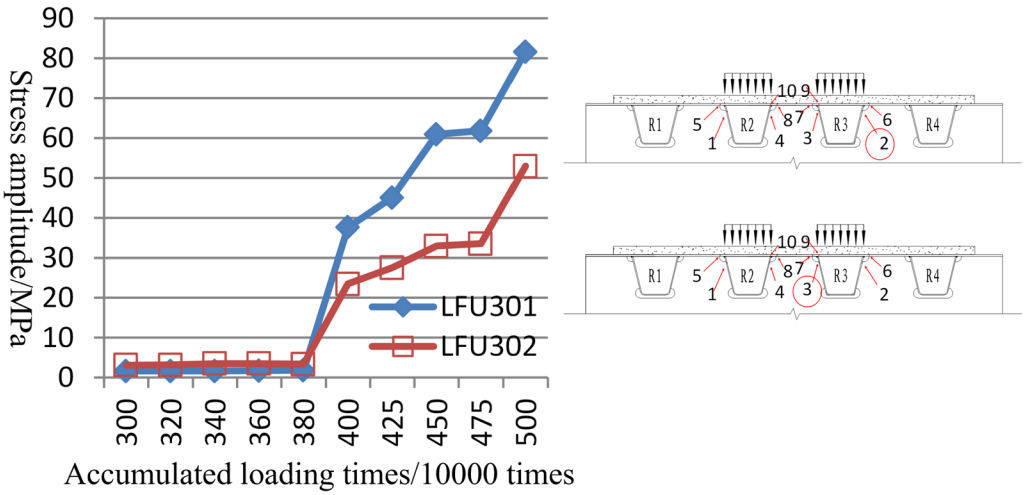

Fig. 25 Stress amplitude variation at target measuring points near R3 rib after composite deck retrofit

two cracks after the retrofit, the crack lengths remained unchanged, indicating that while the structure experienced significant fatigue excitation at these locations, the UHPC layer effectively mitigated its impact on structural damage. These observations suggested that the steel–UHPC composite deck structure effectively restrained further crack degradation and slowed the pace of deterioration on the U-rib wall.

Table 4 compares the worst-case crack dimensions before and after installation of the UHPC overlay. In the unreinforced steel deck, the principal C.6.1 cracks lengthened by more than 20 mm—and DPS01.1 Crack 5 deepened from 2.5 mm to 7.8 mm—within only 0.6 million additional cycles, demonstrating rapid pre-retrofit deterioration. Once the UHPC layer and transverse steel strips were in place, all previously identified cracks either ceased growing or grew imperceptibly during a further two million cycles, even though local stress amplitudes at the tips of Cracks 2 and 3 remained high. Smaller late-stage cracks (e.g., DPS01 and minor DPS01.1) likewise

Table 4 Pre- and post-reinforcement fatigue crack change comparison

Structural type	Crack number	Crack Type	Cumulative loading times/10000	Total cumulative loading times/10000	Maximum crack length/mm	Maximum crack depth/mm	Remarks
Traditional steel bridge deck	1	C.6.1	20	320	172 (↑23)*	6 (through)	Rapidly growing
	4	C.6.1	40	340	146 (↑31)*	6 (through)	
	5	DPS01.1	60	360	135 (↑26)#	7.8 (↑5.3)#	
	8	DPS01.1	20	320	45 (↑18)#	2.6 (↑1.7)#	
	10	DPS01	100	400	62 (↑35.2)#	4.5 (↑2.7)#	
Composite bridge deck	1	C.6.1	200	500	172 (–)	6 (through)	No longer growing
	4	C.6.1	200	500	146 (–)	6 (through)	
	5	DPS01.1	200	500	135 (–)	7.8 (–)	
	8	DPS01.1	200	500	45 (–)	2.6 (–)	
	10	DPS01	200	500	65 (–)	4.5 (–)	
	2	C.6.1	200	500	124 (–)	6 (through)	Stress amplitudes at the crack tips has increased
	3	C.6.1	200	500	112 (–)	6 (through)	
	6	DPS01.1	200	500	45 (–)	1.9 (–)	No longer growing
	7	DPS01.1	200	500	48 (–)	1.5 (–)	
	9	DPS01	200	500	24.3 (–)	1.2 (–)	

* The crack length is the sum of the extension lengths on both sides + the thickness of the partition (8 mm) + the size of the weld toe (6 mm) × 2. 2). #Ultrasound examination results. 3). – indicates no significant changes or unavailability

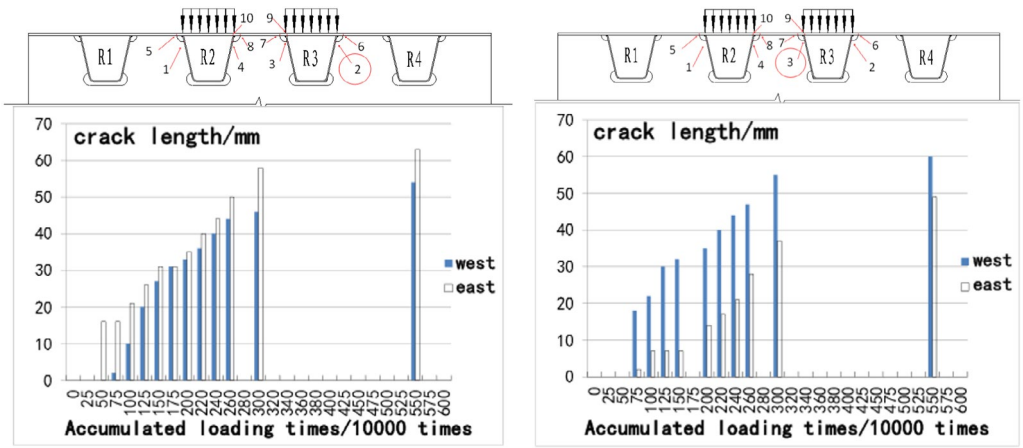

(a) Crack 2. (b) Crack 3.

Fig. 26 Checked result of the crack change at the target loading position

remained stable. Hence the composite steel–UHPC deck effectively arrests crack propagation and provides a substantial margin of fatigue life beyond the original design target.

These findings demonstrate the efficacy of UHPC reinforcement in improving fatigue resistance and mitigating crack propagation, offering valuable insights for the maintenance and reinforcement of similar bridge structures.

4.4.4 Fatigue Safety Verification Stage for Composite Deck

During the 2-million cycle fatigue loading at the diaphragm area, out of a total of 4 to 6 million cycles, regular inspections uncovered 112-mm to 124-mm C.6.1 type cracks (2&3) on rib R3 ceased to extend after reaching a certain length during the 1.5 millionth cycle (Fig. 26). The same type of cracks (1&4), which were about 146–172 mm in length on ribs R2, showed no further growth.

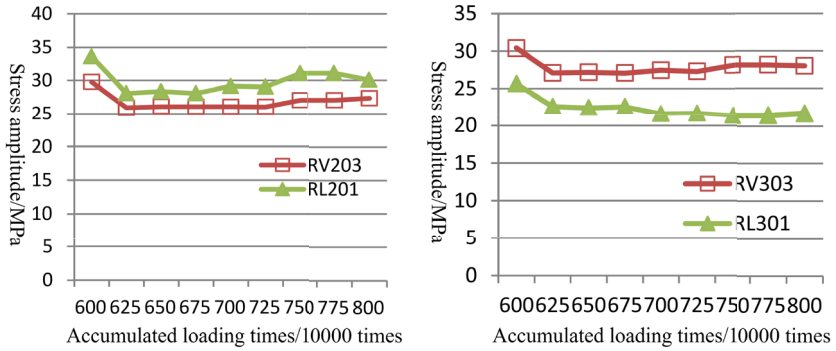

Fig. 27 Stress amplitude changes at fatigue-sensitive details at the U-rib wall end and the diaphragm assembly hole

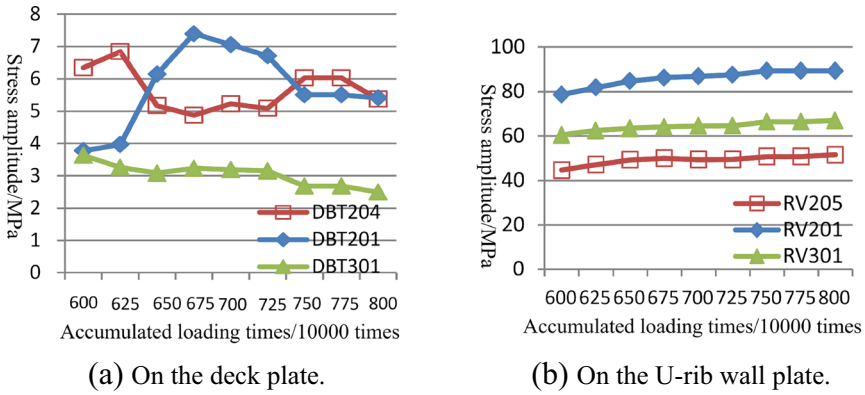

Fig. 28 Stress amplitude changes at fatigue-sensitive details at the mid-span connection between the deck plate and U-rib

In addition, no further deterioration was observed in the deck-plate's existing fatigue cracks (DPS01/DPS01.1), including a significant crack 5 that was 7.8 mm in depth and 135 mm in length. Second, during the first 2 million cycles of loading, no significant changes in stress amplitude were observed at any of the fatigue cracks (Figs. 27, 28, 29 and 30). Compared to the previous two phases, the stress amplitude at DPS01-type fatigue details

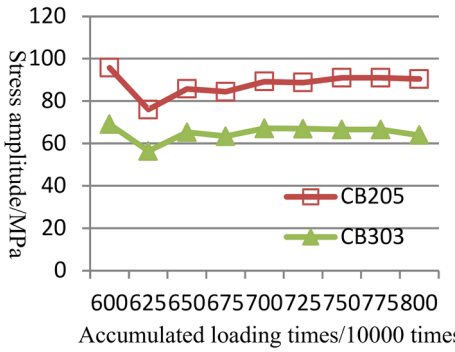

Fig. 29 Stress amplitude changes at fatigue-sensitive details of C.7.1 at the diaphragm assembly hole

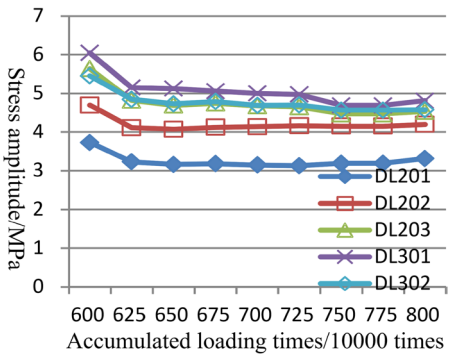

Fig. 30 Stress amplitude changes at target measuring points in the UHPC layer's negative bending moment area throughout the loading cycles

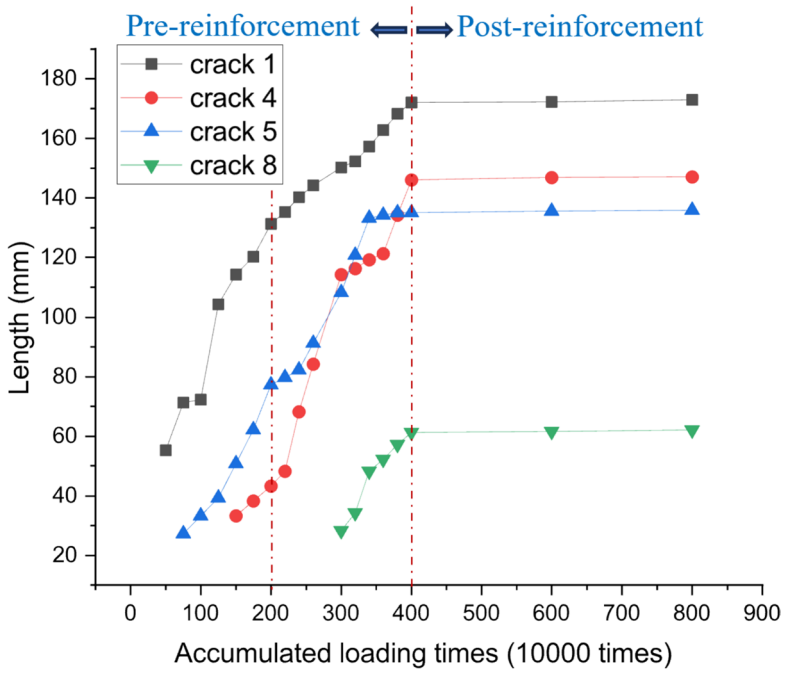

Fig. 31 Progression pattern of crack lengths for C.6.1 and DPS01.1 with cumulative load cycles

decreased by approximately 96%, while the maximum reduction at C.6.1 fatigue details was 57%. These observations validated the enhanced fatigue safety of the sensitive C.6.1 and DPS01.1 details after reinforcement and confirmed the adequacy of the specified repair criteria for deck-plate cracks.

At the end of the 2-million cycle loading in the mid-span area (out of a total of 6–8 million cycles), no fatigue cracks were identified at the fatigue-sensitive details of the deck plate and U-rib connection. Nearby control measuring points also showed no significant changes in stress amplitude (Figs. 28 and 29). This result also validated the safety of the reinforced critical fatigue-sensitive details (C.1 through C.4 and C.7.1).

The changes in stress amplitude at target measuring points in the UHPC layer's negative bending moment area throughout the loading cycles showed no significant variations, indicating the reinforcement's effectiveness in maintaining structural integrity under fatigue loading (Fig. 30).

Collectively, these results confirmed the improved fatigue safety of the Junshan Yangtze River Bridge by the steel–UHPC composite deck structure at all fatigue-sensitive details (C.1 through C.7 and DPS01) and the UHPC layer throughout its design life.

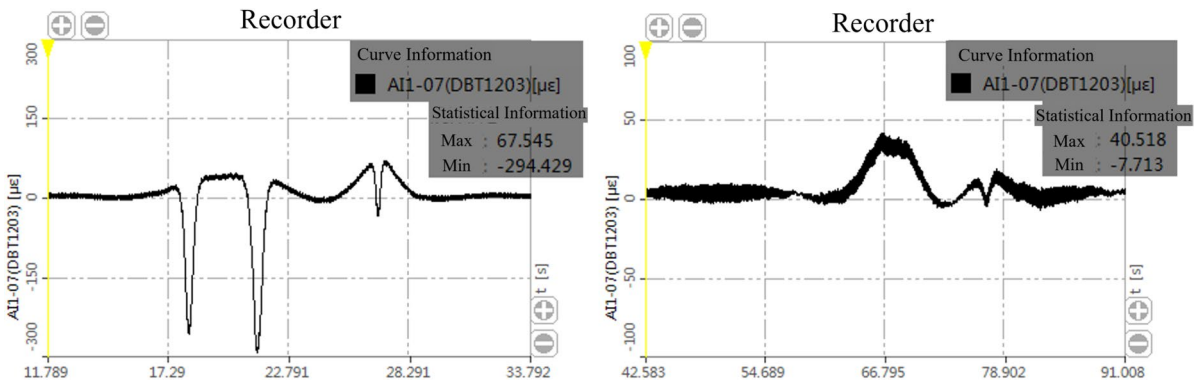

Fig. 32 Strain progression of DBT series target measuring points on the underside of the top plate of the Junshan Yangtze River Bridge, pre- and post-reinforcement

4.5 Overall Analysis

From the experimental observations described earlier, it is evident that after the specimen underwent 8 million cycles of loading at the diaphragm location, three types of fatigue cracks emerged at the connection points of the top plate, U-rib, and diaphragm. These cracks include C.6.1 (Cracks 1, 2, 3, 4), DPS01.1 (Cracks 5, 6, 7, 8), and DPS01 (Cracks 9, 10), which are among the most frequent and detrimental fatigue cracks in orthotropic steel bridge decks.

Due to the internal positioning of DPS01-type cracks, their length is difficult to measure, and the data are incomplete. Therefore, when studying the effect of the UHPC layer reinforcement on crack propagation rate, only C.6.1 and DPS01.1 cracks are considered. Figure 31 illustrates how the length of these two types of cracks changes with the number of load cycles.

From the figure, it can be observed that, first, C.6.1 type cracks generally initiate earlier than DPS01.1 type cracks, indicating that the U-rib web is more prone to cracking compared to the deck plate. Second, before UHPC reinforcement, both types of cracks initially exhibit a rapid increase in length, which is then followed by a slower growth phase. The first point of significant change in propagation rate occurs at approximately 2 million cumulative load cycles. This indicates that the rate of deterioration for both types of fatigue cracks remain generally consistent within the designed service life of the bridge. After exceeding the design service life, the rate of stiffness deterioration in the bridge shows a relatively deceleration.

Nevertheless, even after twice the design service life of the bridge, it is not too late to apply the reinforcement method proposed in this study to the steel bridge deck. After an additional 4 million load cycles, regardless of whether the axle load was applied at the diaphragm or mid-span, the two types of cracks exhibited almost no further growth. This demonstrates that the proposed reinforcement and retrofitting method for severely cracked orthotropic steel bridge decks is effective.

4.6 Analysis of In-Situ Measurements on a Real Bridge Results on the Junshan Yangtze River Bridge

Fig. ure 32 shows the strain progression at the DBT series transverse measuring points on the underside of the top plate of the Junshan Yangtze River Bridge before and after reinforcement using the UHPC layer, under the same driving conditions. To analyze the changes in fatigue performance of this measuring point post-retrofit, the nominal stress method was employed. Using Hooke's Law, the stress amplitudes before and after the retrofit were calculated to be 74.55 MPa and 9.9 MPa, respectively.

This indicates that, under the constraints of the UHPC layer, the stiffness of the bridge deck significantly increased after the retrofit. The nominal stress amplitude dropped to approximately 13% of the original value, demonstrating a substantial improvement in fatigue resistance, which greatly extends the service life of the original bridge. This method proves to be an effective reinforcement approach for heavily cracked orthotropic steel bridge decks.

5 Main Conclusions

This study conducted fatigue performance tests on the orthotropic steel bridge deck of the Junshan Yangtze River Bridge, which was reinforced with a UHPC layer containing transverse steel-plate strips. The findings suggest that the reinforcement enhanced fatigue performance and assured fatigue safety, making it a reinforcement and rehabilitation technology worth promoting for severely cracked orthotropic steel bridge decks. In addition, the comparative data were validated for accuracy.

First, the steel–UHPC composite bridge deck structure significantly improves the fatigue performance of the orthotropic steel deck, delaying the initiation and propagation of cracks and thereby extending the deck's fatigue life. Second, a comparative analysis of the laboratory-test model data before and after fatigue loading validates that the UHPC layer reinforcement substantially enhances the steel deck's fatigue resistance. This effect is particularly pronounced at fatigue-sensitive detail locations of DPS01/DPS01.1 and C.6.1 (stress amplitude reduction of up to 96% at DPS01/DPS01.1 type fatigue details, and up to 57% at C.6.1 type fatigue details). Finally, the third phase fatigue laboratory fatigue test results confirm that the fatigue safety of the reinforced steel–UHPC composite bridge deck structure is assured throughout its designed service life. Furthermore, the in-situ measurements on a real bridge results on the Junshan Yangtze River Bridge also show that, compared to the pre-reinforcement state, the stress amplitude at the measurement points at the connection between the top plate, U-rib, and transverse diaphragm decreased by 86% after reinforcement, which is significant, because these locations are the most prone to cracking in orthotropic steel bridge decks. These findings offer robust technical support for similar maintenance and reinforcement projects on other bridges.

Overall, the UHPC layer reinforcement emerges as an effective method to improve the fatigue performance of orthotropic steel bridge decks and holds significant practical importance for extending bridge service lives and ensuring traffic safety. Future research directions could further optimize UHPC's material mix,

reinforcement layer design parameters, and long-term performance evaluation of the reinforcement effect to enhance the cost-effectiveness and applicability of the reinforcement technology.

Acknowledgements
The authors express their gratitude to Shanghai Zhenhua Heavy Industries Co., Ltd. for technical support in fabricating the laboratory-test specimen, and to the Wuhan R&D Center for providing fatigue testing equipment.

Author contributions
Zengkui Xie: experimental design, data analysis, and manuscript writing. Zhilin Chen: data organization and figure creation. Chenhui Zhu: project management. Zhongsong SU: test preparation and equipment setup. Lipo Yang: overall research guidance and manuscript revisions. Wei Zou: numerical simulations and experimental validation.

Funding
This research was supported by the following projects: Zhejiang Provincial Department of Education Research Project (Project ID: Y202456708). Jiaxing Vocational Technical College Institution-Sponsored Research Project (Project ID: 2024024). Tianjin Transportation Commission and Tianjin Municipal Engineering Design & Research Institute (Grant No.: 2019B-26).

Data Availability
The data and materials used in this study are available upon reasonable request from the corresponding author.

Declarations

Ethics Approval and Consent to Participate
This study does not involve experiments on humans or animals, and therefore, ethics approval is not required. All authors have agreed to participate in this research and support its publication.

Consent for Publication
All authors have reviewed and approved the submission of this manuscript to the International Journal of Concrete Structures and Materials.

Competing Interests
The authors declare that there are no competing interests.

Author details
[1]School of Urban Construction, Jiaxing Vocational Technical College, Jiaxing 314036, China. [2]Guangdong Provincial Highway Construction Co., Ltd, Guangzhou 510000, China. [3]CCCC Highway Bridges National Engineering Research Centre Co., Ltd., Beijing 100088, China. [4]Guangzhou Highway Engineering Group Co., Ltd., Guangzhou 510180, China. [5]Tianjin Municipal Engineering Design & Research Institute, Tianjin 300392, China.

Received: 14 January 2025 Accepted: 26 June 2025
Published online: 11 September 2025

References

Abdelbaset, H., Tian, L., & Zhao, J. (2022). Steel-UHPC composite deck Rib-to-floorbeam connection fatigue resistance fatigue life crack propagation. *Structures, 36*, 153–167. https://doi.org/10.1016/j.istruc.2021.12.008

Aizhu, Z. (2017). Full scale model fatigue test of orthotropic steel bridge deck with inner partition. *Steel Structure*. https://doi.org/10.13206/j.gjg201701010

ASHTO. (2012). *AASHTO LRFD bridge design specifications* (6th ed.). AASHTO.

Bing, C., Jingquan, W., & Jiaping, L. (2023). Research progress and scale application technology path analysis of UHPC bridges. *Chinese Journal of Highways, 36*(9), 1–19. https://doi.org/10.19721/j.cnki.1001-7372.2023.09.001

BS EN 1993-1-9:2005 Eurocode 3: Design of steel structures. Part 1–9: fatigue. London, UK: British StandardsInstitution, 2005

Chen, Q. (2015). Research on fatigue performance and maintenance reinforcement methods of orthotropic steel bridge decks. Beijing Jiaotong University

Chunsheng, W., Bingning, F., Qin, Z., & Yacheng, F. (2013). Full scale fatigue test of orthotropic steel bridge deck panels. *Chinese Journal of Highways, 26*(2), 69–76. https://doi.org/10.19721/j.cnki.1001-7372.2013.02.011

Dieng, L., Marchand, P., Gomes, F., Tessier, C., & Toutlemonde, F. (2013a). Use of UHPFRC overlay to reduce stresses in orthotropic steel decks. *Journal of Constructional Steel Research, 89*, 30–41. https://doi.org/10.1016/j.jcsr.2013.06.006

Dieng, L., Marchand, P., Gomes, F., Tessier, C., & Toutlemonde, F. (2013b). Use of UHPFRC overlay to reduce stresses in orthotropic steel decks. *Journal of Constructional Steel Research, 09*, 30–41. https://doi.org/10.1016/j.jcsr.2013.06.006

Dong, J., Liu, Y., Wang, Z., et al. (2020). Fatigue assessment of orthotropic steel bridge decks based on long-term wheel loading. *Engineering Structures, 219*, 111437. https://doi.org/10.1016/j.engstruct.2020.111437

EN 1993-2:2006 Eurocode 3: Design of steel structures. Part 2: steel bridges. Brussels: European Committee for Standardization, 2006.

Fu, Z. Q., Ji, B. H., Xie, S. H., & Liu, T. J. (2017). Crack-stop holes in steel bridge decks: Drilling method and effects. *Journal of Central South University, 24*(10), 2372–2381. https://doi.org/10.1007/s11771-017-3649-8

Hanyong, L., Long, Li., & Hedong, Li. (2019). Mechanical performance analysis and fatigue test of steel ultra high ductility concrete composite bridge deck structure. *Highway Transportation Technology, 36*(08), 59–66. https://doi.org/10.3969/j.issn.1002-0268.2019.08.008

Hou, M., Lee, S., Kim, D., et al. (2025). Fatigue performance of ultra-high-performance concrete (UHPC): A literature review. *Journal of Materials Research and Technology, 27*, 1042–1063. https://doi.org/10.1016/j.jmrt.2025.01.117

Huang, W., Lin, G., Qian, Z., & Liu, Z. (2006). Fracture mechanics analysis of fatigue life of orthotropic steel bridge deck pavement layer. *China Civil Engineering Journal, 9*, 112–116. https://doi.org/10.3321/j.issn:1000-131X.2006.09.019

Japanese Road Association (2012). Road and Bridge Rules. With Interpretation. Tokyo: Marubeni Publishing Division.

Junhui, C., Wei, F., Lifeng, L., Xudong, S., Yang, Z., & Hua, Z. (2022). Research and application of high performance bridge structures based on UHPC. *Journal of Hunan University (Natural Science Edition), 49*(11), 1–32. https://doi.org/10.16339/j.cnki.hdxbzkb.2022114

Junhui, C., Yuhang, Z., Xudong, S., & Xiujiang, S. (2022). Experimental study on bending fatigue and residual bearing capacity of steel thin layer UHPC lightweight composite bridge deck structures. *Journal of Hunan University, 49*(11), 89–104. https://doi.org/10.16339/j.cnki.hdxbzkb.2022120

Kim, J. S., Kwark, J., Joh, C., Yoo, S. W., & Lee, K. C. (2015). Headed stud shear connector for thin ultra-high-performance concrete bridge deck. *Journal of Constructional Steel Research, 108*, 23–30. https://doi.org/10.1016/j.jcsr.2015.02.001

Li, M. (2018). Fatigue life and reliability study of welded details of steel bridge decks under random vehicle loads. *Changsha University of Science and Technology*. https://doi.org/10.26985/d.cnki.gcsjc.2018.000001

Liang, T., Liji, H., Gao, L., Chunsheng, W., & Bingning, F. (2014). Fatigue testing of full-scale models of orthotropic steel bridge decks. *Journal of Civil Engineering, 47*(3), 112–122. https://doi.org/10.15951/j.tmgcxb.2014.03.006

Libing, Z., Gang, Z., & Min, W. (2020). Research on the effect of steel UHPC composite deck renovation of Junshan Yangtze River Bridge. *Bridge Construction, 50*, 49–54. https://doi.org/10.3969/j.issn.1003-4722.2020.02.009

Ling, L., & Tang, L. (2018). Fine finite element analysis of hot spot stress in welded joints of steel bridge deck Top-U Rib. *Highway Traffic Science and Technology, 4*, 58–66. https://doi.org/10.3969/j.issn.1002-0268.2018.04.008

Qin, S., Yu, L., Zhang, J., & Gao, L. (2022). Fatigue assessment of steel–UHPC composite deck with a thin polymer overlay in a long-span suspension bridge under static and random traffic loads. *International Journal of Fatigue, 168*, 107409. https://doi.org/10.1016/j.ijfatigue.2022.107409

Qin, S., Zhang, J., Huang, C., Gao, L., & Bao, Y. (2022). Fatigue performance evaluation of steel-UHPC composite orthotropic deck in a long-span cable-stayed bridge under in-service traffic. *Engineering Structures, 254*, 113875. https://doi.org/10.1016/j.engstruct.2022.113875

Qinghua, Z., Chuang, C., Yizhi, B., & Qiao, L. (2014). Study on fatigue characteristics of orthotropic steel bridge decks for Hong Kong Zhuhai Macao Bridge. *Journal of Civil Engineering, 47*(9), 110–119. https://doi.org/10.15951/j.tmgcxb.2014.09.039

Qinghua, Z., Yiming, L., & Yizhi, B. (2017). Study on fatigue performance of orthotropic composite bridge decks with large longitudinal ribs. *Chinese Journal of Highways, 30*(3), 226–235. https://doi.org/10.3969/j.issn.1006-3897.2017.03.025

Radaj, D., Sonsino, C. M., & Fricke, W. (2009). Recent developments in local concepts of fatigue assessment of welded joints. *International Journal of Fatigue, 31*, 2–11. https://doi.org/10.1016/j.ijfatigue.2008.05.019

Ren, W., Li, X., & Li, J. (2007). Analysis of fatigue problems in modern highway steel bridge typical details. *Highway, 4*, 82–87.

Samol, Y., & Yamada, K. (2008). Fatigue durability evaluation of trough to deck plate welded joint of orthotropic steel deck. *Structural Engineering and Earthquake Engineering, JSCE, 25*(2), 33s–46s. https://doi.org/10.2208/jsceja.64.603

Shao, X., Zhou, H., & Cao, J. (2013). Shear performance of welded studs in steel-thin-layer RPC composite bridge deck structure. *Highway Traffic Science and Technology, 04*, 34–39. https://doi.org/10.3969/j.issn.1002-0268.2013.04.007

Shi, Z., Su, Q., Kavoura, F., & Veljkovic, M. (2022). Fatigue behaviour evaluation of full-scale OSD–UHPC composite bridge deck system. *Engineering Structures, 275*, 115179. https://doi.org/10.1016/j.engstruct.2022.115179

Shili, Y., & Zhou, S. (2017). Research status of fatigue damage in orthotropic steel decks of large-span steel box girder bridges in China. *Bridge Construction, 47*(4), 60–65. https://doi.org/10.3969/j.issn.1003-4722.2017.04.011

Short Span Steel Bridge Alliance. (2020). Sandwich Plate System (SPS) Deck. https://shortspansteelbridges.org/wp-content/uploads/2020/07/SPS-Deck-Tech-Note.pdf

Standards of the People's Republic of China: Code for Design of Highway Steel Bridges JTG D64-2015. 2015.

Shao X, Deng L, Cao J. Innovative steel-UHPC composite bridge girders for long-span bridges[J]. Frontiers of Structural and Civil Engineering, 2019, 13(4): 981–989. https://doi.org/10.1007/s11709-019-0531-9

Tang, L., Huang, L., Liu, G., et al. (2012). Study on fatigue cracks in top plate of orthotropic steel bridge deck. *Highway Traffic Science and Technology, 02*, 63–70. https://doi.org/10.3969/j.issn.1002-0268.2012.02.011

Tang, L., Huang, L., Liu, G., et al. (2014). Fatigue test of full-scale model of orthotropic steel bridge deck. *China Civil Engineering Journal, 3*, 112–122. https://doi.org/10.15951/j.tmgcxb.2014.03.006

Wang, Q. (2019). Evaluation and prediction of typical fatigue damage of orthotropic steel bridge deck. Beijing University of Civil Engineering and Architecture

Wang, Y., Shao, X., Chen, J., Cao, J., & Deng, S. (2021). UHPC-based strengthening technique for orthotropic steel decks with significant fatigue cracking issues. *Journal of Constructional Steel Research, 176*, 106393. https://doi.org/10.1016/j.jcsr.2020.106393

Wei, C., Zhang, Q., Yang, Z., Li, M., Cheng, Z., & Bao, Y. (2022). Flexural cracking behavior of reinforced UHPC overlay in composite bridge deck with orthotropic steel deck under static and fatigue loads. *Engineering Structures, 265*, 114537. https://doi.org/10.1016/j.engstruct.2022.114537

Xiang, Z., & Zhu, Z. (2021). Simulation study on fatigue behavior of wrap-around weld at rib-to-floorbeam joint in a steel-UHPC composite orthotropic bridge deck. *Construction and Building Materials, 289*, 123161. https://doi.org/10.1016/j.conbuildmat.2021.123161

Xin, H., Correia, J. A. F. O., & Veljkovic, M. (2021). Three-dimensional fatigue crack propagation simulation using extended finite element methods for steel grades S355 and S690 considering mean stress effects. *Engineering Structures, 227*, 111414. https://doi.org/10.1016/j.engstruct.2020.111414

Xiong, J., Ye, Y., & Yu, T. (2003). Fatigue life evaluation of orthotropic steel bridge decks. *World Bridges, 3*, 24–27. https://doi.org/10.3969/j.issn.1671-7767.2003.03.008

Xiong, Z., Wang, D., Xiang, C., et al. (2021). Experimental study on root-deck fatigue cracks in orthotropic steel decks. *Materials & Design, 203*, 109601. https://doi.org/10.1016/j.matdes.2021.109601

Xudong, S., & Junhui, C. (2017). Research and application of high performance bridge structures for the future. *Journal of Building Science and Engineering, 34*(5), 42–58. https://doi.org/10.3969/j.issn.1673-2049.2017.05.005

Xudong, S., & Minghong, Q. (2019). Research and development of high performance prefabricated bridge structures based on UHPC materials. *Journal of xi'an University of Architecture and Technology (Natural Science Edition), 51*(2), 160–167. https://doi.org/10.15986/j.1006-7930.2019.02.002

Xudong, S., Minghong, Q., Banfu, Y., & Jun, L. (2017). Research and application progress of ultra high performance concrete in bridge engineering at home and abroad. *Materials Introduction, 23*, 33–43. https://doi.org/10.11896/j.issn.1005-023X.2017.023.004

Xudong, S., Zhe, Z., & Menglin, L. (2012). Experimental study on the flexural tensile strength of orthotropic steel-RPC composite bridge decks. *Journal of Hunan University, 39*(10), 8–13. https://doi.org/10.3969/j.issn.1674-2974.2012.10.002

Yang, L., Dan, Z., Lei, C., & Wang, D. (2021). Research progress on steel-UHPC composite structure bridges. *Materials Introduction, 35*, 3104–3113. https://doi.org/10.11896/cldb.19090024

Yang, W., Xudong, S., Jie, C., Junhui, C., & Liguo, W. (2020). UHPC reinforcement technology for steel bridge decks with severe fatigue cracking. *Journal of Civil Engineering, 53*, 92–101115. https://doi.org/10.15951/j.tmgcxb.2020.11.010

Yiming, L. (2019). Research on fatigue failure mechanism of large longitudinal rib orthotropic steel-UHPC composite bridge deck Southwest Jiaotong University. https://doi.org/10.27414/d.cnki.gxnju.2019.001887

Zhang, Q., Bu, Y., & Li, Q. (2017). Research progress on fatigue problems of orthotropic steel bridge decks. *China Journal of Highway and Transport, 30*(03), 14–30. https://doi.org/10.19721/j.cnki.1001-7372.2017.03.002

Zhang, T., Fang, L., Fu, Z., & Ji, B. (2019). Steel plate reinforcement of orthotropic bridge decks. *Journal of Constructional Steel Research, 162*, 105747. https://doi.org/10.1016/j.jcsr.2019.105747

Zhang, W., Liu, H., Li, H., et al. (2022). Fatigue performance evaluation of steel–UHPC composite deck on the Junshan Yangtze River Bridge. *Journal of Constructional Steel Research, 192*, 106946. https://doi.org/10.1016/j.jcsr.2022.106946

Zhu, Z., Zhu, R., & Xiang, Z. (1906). A review on behavior and fatigue performance of orthotropic steel–UHPC composite deck. *Buildings, 13*, 1906. https://doi.org/10.3390/buildings13081906

Publisher's Note

Zengkui Xie Assistant Researcher, School of Urban Construction, Jiaxing Vocational Technical College

Zhilin Chen Engineer, Guangdong Provincial Highway Construction Co., Ltd.

Chenhui Zhu Assistant Engineer, CCCC Highway Bridges National Engineering Research Centre Co., Ltd.

Zhongsong Su Engineer, Guangzhou Highway Engineering Group Co., Ltd.

Lipo Yang Professor-level Senior Engineer, Tianjin Municipal Engineering Design & Research Institute

Wei Zou Engineer, Guangdong Provincial Highway Construction Co., Ltd.